Kinetics and Muscle Modeling of a Single Degree of Freedom Joint
Part II: Spindles and Sensory Neurons

Rick Wells
Aug. 13, 2003

I. The Hill Model for Intrafusal Fiber

The second part of this tech brief deals with modeling the intrafusal muscle fibers and the sensory neurons. We begin with the mechanical model of the intrafusal muscle fibers. From the "Muscles" tech brief we recall that intrafusal fibers are too weak to play any mechanical role in the force exerted by a muscle. Instead their role has been described as that of a "sophisticated strain gauge." Figure 1, taken from Matthews[1], is an illustration of a muscle spindle. A muscle spindle contains two major components: the bag and/or chain fibers, which are innervated by axons from gamma motoneurons and contain contractile elements; and the receptor tissues in which are intertwined nerve ends from the primary (group Ia) or secondary (group II) sensory neurons. Spindle fibers are generally a few mm in length, with large ones sometimes exceeding 10 mm, and they are attached to in parallel to the extrafusal fibers. They are thus subject to the same stretch (or contraction) as the whole muscle. The portion of the spindle containing the receptor makes up about one to two tenths of the total resting length of the spindle.

A more detailed look at the receptor structure is illustrated in Figure 2. Bag fibers (whose receptors are primary sensors, i.e. group Ia) and chain fibers (whose receptors are both primary and secondary sensors, i.e. group II) are arranged in parallel with each other. Although this illustration seems to imply that the same gamma motoneuron axon innervates both types, this is not the case. Dynamic and static gamma MNs separately innervate the two types.

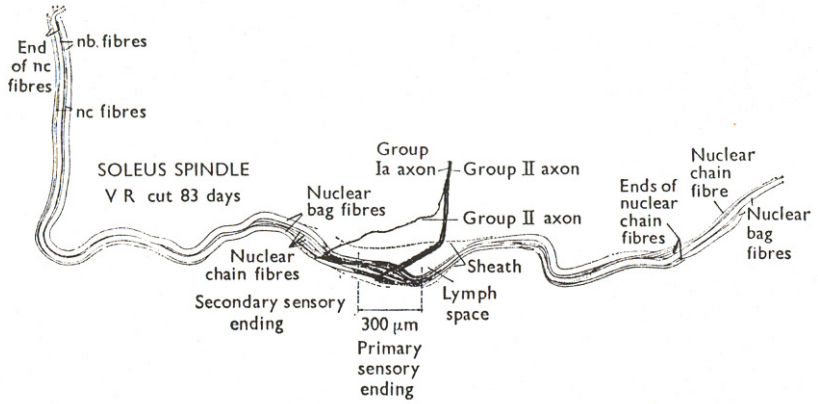

Figure 1: Illustration of a cat muscle spindle. The figure is drawn to scale. Efferent axons from gamma motoneurons are not shown in this figure, but they extensively innervate the nuclear bag fibers and nuclear chain fibers in the spindle. Muscle spindle fibers (= intrafusal fibers) are a few mm in length with some large fibers exceeding 10 mm in length. The central portion of the spindle, making up about one to two tenths of its relaxed length, contains the nerve endings for the group Ia and group II sensory neurons.

[1] P.B.C. Matthews, *Mammalian Muscle Receptors and Their Central Actions*, London: Edward Arnold, 1972.

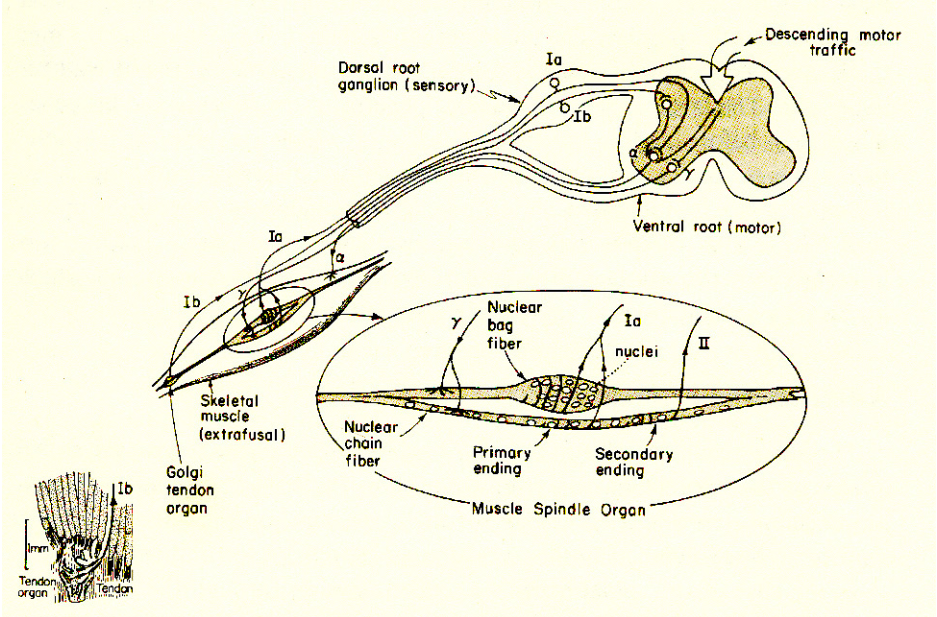

Figure 2: Detailed look at the structure of the muscle spindle. The intrafusal spindle fibers are embedded with extrafusal motor units, although the spindle itself is driven by gamma motoneurons and therefore constitutes its own "gamma motor unit" separately from the extrafusal motor unit. Bag 1 fibers are innervated by dynamic γ-MNs; bag 2 and chain fibers are innervated by static γ-MNs. We can therefore say that the bag fibers and the chain fibers constitute their own separate spindle motor units. This figure is taken from McMahon.[2]

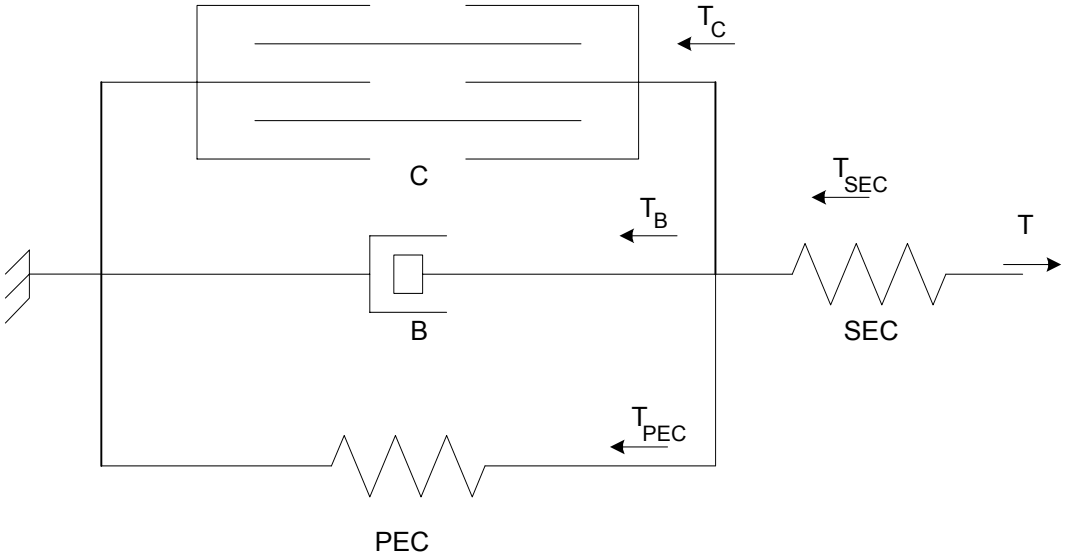

Figure 3: Hill model for intrafusal spindle fiber. This model is in the second of the two canonical forms for the Hill model. C = contractile element; B = damper element; PEC = parallel elastic component; SEC = series elastic component. x_p is the length of the parallel arrangement C + B + PEC; x_s is the length of the SEC. Total spindle length is $\lambda = x_p + x_s$. The SEC represents the part of the spindle containing the roots of the sensory neuron.

[2] T.A. McMahon, *Muscles, Reflexes, and Locomotion*, Princeton, NJ: Princeton University Press, 1984.

The usual approach to modeling the spindle is via the Hill model, illustrated in Figure 3. The model represents one spindle, either a bag fiber (containing group Ia sensors) or a chain fiber (containing group II and group Ia sensors), but not both. We can say that the model of figure 3 makes up its own complete intrafusal motor unit (no addition parallel contractile elements).[3] I should mention that figure 3 is in the second canonical form of the Hill model, and this is why it is drawn differently from the Hill model of part I of this brief.

Although it would be natural to assume that the mathematical model of the intrafusal spindle elements is exactly the same as for the extrafusal muscle case, this would be misleading and not strictly true. For one thing, in a muscle at its normal resting position the intrafusal fibers are already in extension beyond their slack length. Thus, both the SEC and the PEC are taut at the normal resting length of the muscle, and therefore they both contribute to tension in the fibers. For another thing, SEC and PEC have more clear-cut physical interpretations in the spindle. The PEC is associated with the nuclear fibers (bag or chain), while the SEC is associated with the receptor area containing the sensory nerve endings. This is the main reason we use the second canonical form of the Hill model for the intrafusal muscle spindle. A third difference is that the length λ of the spindle is not necessarily the same as the overall muscle length ℓ, although it is certainly related to it. The difference is made up by the connective tissue that attaches them at both ends to the main extrafusal muscle mass. We regard the stiffness of this connective tissue as being much greater than that of the spindle fibers, and therefore as not contributing to the dynamics of the spindle. We can therefore say that muscle length and spindle length are related as

$$\ell = \ell_c + \lambda = \ell_c + x_p + x_s \tag{1}$$

where ℓ_c is the length of the connective tissue, x_p is the length of the contractile element (and also of the PEC), and x_s is the length of the SEC. We take ℓ_c as a fixed constant provided that the spindle is not slack. (If it is slack, then the connective tissue is slack, too).

A spindle typically contains two bag fibers and three to five chain fibers. Intrafusal muscle fiber diameters vary from 6 to 28 μm in diameter. The total number of spindles in a muscle varies, numbering about 70 in the medial gastrocnemius muscle of the cat[1]. Mechanically speaking, it is probably not correct to try to assign spindles to particular individual extrafusal motor units, i.e. not correct to say "this is the spindle for that extrafusal motor unit". On the other hand, as we saw in the "Muscles" tech brief a spindle does share innervation by beta motoneurons with some extrafusal muscle fibers. In this sense the spindles may be "electrically paired up" with particular extrafusal motor units. But because each spindle contains multiple bag and chain fibers, the spindle is probably "paired" with multiple extrafusal motor units, each "pair" being comprised of one bag-or-chain fiber and one extrafusal motor unit.[4] If this is so, it would permit monitoring of the individual extrafusal motor units by their own spindle sensor via the "task group" concept introduced in part I of the spinal sensorimotor system tech brief.

Unlike the extrafusal muscle fibers, the viscoelastic properties of intrafusal fibers seem to be much less studied. At least, I haven't yet found any sources in the literature where these

[3] I should point out that our concept of a motor unit is made a bit ambiguous by the existence of beta motoneurons. We defined the motor unit concept as "one motoneuron drives one motor unit". However, the beta motoneurons "parallel" the actions of alpha- and gamma-motoneurons in the muscle, as we showed in the "Muscles" tech brief. Hence, when we talk about the tension Q_C of the contractile unit, we must regard its action potential input as the sum of contributions from the main motoneuron and the beta motoneuron.
[4] I'm speculating here. I have no evidence from reference material to back this up.

properties have been examined in the kind of detail that I've found for the extrafusal fibers. The types of mechanical experiments conducted on extrafusal fibers do not work so well for intrafusal fibers because the intrafusal fibers do not directly contribute to the mechanical forces that move limbs. It may be that the information is hiding out there in the literature jungle someplace, but if so I haven't found it yet. Consequently, I have seen no experimental evidence to indicate whether the element laws for figure 3 mirror those of the extrafusal fibers or not.

Indirect evidence does exist that illuminates some of the intrafusal viscoelastic properties. This evidence is gathered from experiments where various stretch patterns have been applied to muscle and the response of the primary (group Ia) and secondary (group II) afferents has been measured. Studies like this can and do tell us some important things about the spindle system, but the data nonetheless confounds mechanical and neuronal information in the observable outputs, thus leaving us with what systems theorists commonly call an "observability" problem. Matthews illustrates this problem as shown in Figure 4.[5] For many types of mechanical stimuli the electrical response of the afferents more or less follows the mechanical input. One possibility is that the overall system might obey a linear and time invariant system model with discrepancies being caused by the stimulus vs. firing rate characteristics of the sensory neurons. But another possibility is that mechanical nonlinearities in the element laws might be "compensated for" by an inverse nonlinearity in the sensory neuron response. I wish to note that where Matthews refers to "adaptation" in figure 4, he uses the word "adaptation" in a different sense than neural network theory uses the word. Matthews and many other biologists use "adaptation" to mean "transient response", which is quite a different thing than "adaptation" in neural network theory.

There is some reason to think that fusimotor activity (i.e. action potential firing by gamma motoneurons) may affect the mechanical properties of the intrafusal fibers. So far as I have been able to find out, this is still an open question. Owing to reliable data to the contrary, we will make

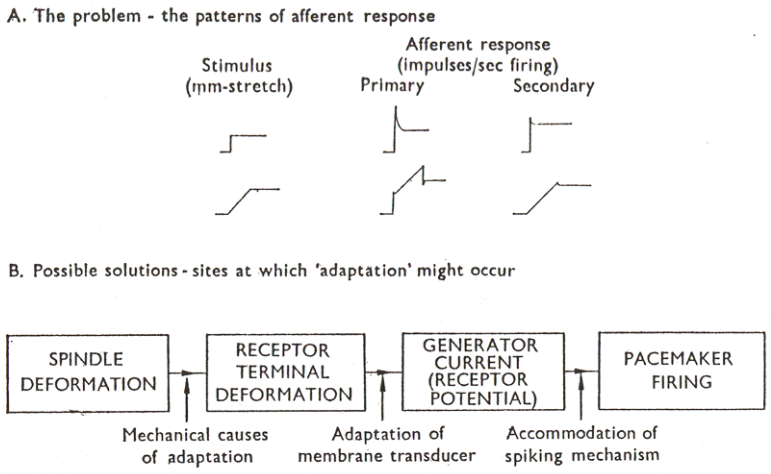

Figure 4: Cascaded factors in mechanical-to-electrical response of spindles. Mechanical deformation of the intrafusal fibers leads to mechanical deformation of receptor nerve endings. This produces an electrical response in the nerve that stimulates afferent firing. For many types of stimuli the electrical response seems to follow the mechanical input. However, it is not clear whether this is because the cascaded system obeys a linear and time invariant model or because nonlinearities in one block are compensated by an inverse nonlinearity in the subsequent blocks.

[5] *op. cit.* Matthews, pg. 265, fig. 6.1.

the assumption that the elements in Hill's model follow the classical laws of a linear spring-damper system. Thus,

$$T_{SEC} = K_{SEC} \cdot (x_s - x_{rs}) \cdot u(x_s - x_{rs}) \quad (2a)$$

$$T_{PEC} = K_{PEC} \cdot (x_p - x_{rp}) \cdot u(x_p - x_{rp}) \quad (2b)$$

$$T_B = B \cdot \dot{x}_s \cdot u(x_s - x_{rs}) \quad (2c)$$

where x_{rs} and x_{rp} are the slack lengths for the SEC and PEC, respectively. For mathematical convenience, we will lump the slack lengths into the connective tissue length term in (1) and set x_{rs} and x_{rp} to zero in equations (2).

As for the contractile element, the microscopic biology of intrafusal muscle has the same generic character as found in extrafusal muscle fibers. This would argue in favor of using the same contractile element law (with different constants, of course) as we saw in part I of this tech brief. It would also plausibly argue that Hill's equation relating velocity and fiber tension should likewise apply, in which case (2c) above would not be correct. However, I am not in possession of any experimental data that would allow me to "put the numbers" in such a model. What we shall do instead is propose a simpler first-order model and then note some of the known departures from what would be predicted by this model. Accordingly, we will propose

$$T_C = Q_C(t) \quad (3a)$$

$$\dot{Q}_C = -\frac{1}{\tau} Q_C + \frac{C_0}{\tau} p(t) \quad (3b)$$

which is the same model as we used in part I of this tech brief but neglects the length modifier function A we used there. There should probably be an A term in our intrafusal fiber model, but it is here where I lack sufficient data to fit a response characteristic curve. This is a rather serious omission in the case of bag fibers (as I will further discuss), but perhaps not so much so for chain fibers.

It is known that there are nonlinear departures from the predictions of these linear models. We need to take a look at what some of the more important of these are. The first is the observation of mechanical "creep" in bag 1 ("dynamic bag") fibers.[6] This is illustrated in Figure 5.[7] At the time of this experiment, the distinction between bag 1 and bag 2 fibers had not yet been made. It is now known that this effect is found in bag 1 but not bag 2 fibers. The creep phenomenon is located in the equatorial region of the spindle (i.e., it is in the SEC). The magnitude of the effect is about 2 to 3% of the total length change, and for purposes of our work this is probably a negligible effect.

A much more serious nonlinearity shows up in the amplitude dependence of primary afferent firing rate (group Ia afferents). Figure 6 illustrates the effect.[8] A sinusoidal stretch at a frequency of 1 Hz was applied to the fibers and the average firing rate of the afferents was measured. The primary afferent (group Ia) had a limited linear range with a high gain in the firing rate vs. length response. After this it exhibited a saturating nonlinearity. The secondary (group II) afferent had a

[6] Recall from the "Muscles" tech brief that there are two kinds of nuclear bag fibers, denoted as "bag 1" or "dynamic" bag fibers and "bag 2" or "static" bag fibers.
[7] *op. cit.* Matthews, pg. 272, fig. 6.5.
[8] *op. cit.* Matthews, pg. 177, fig. 4.22.

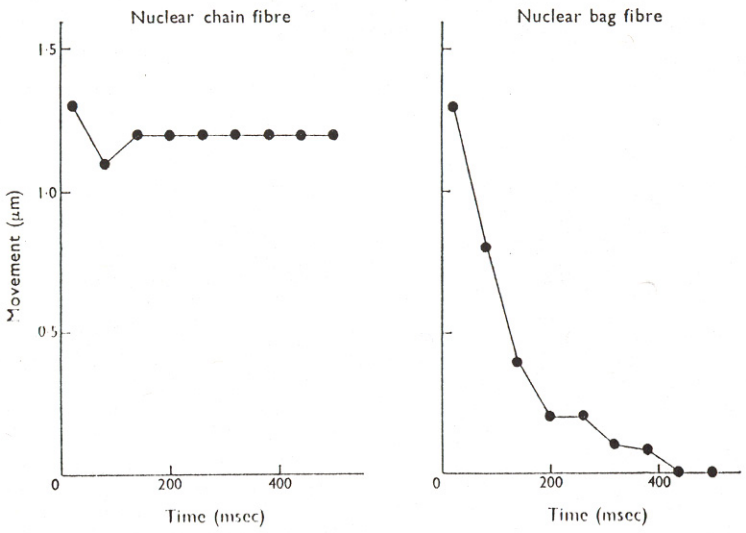

Figure 5: "Creep" in bag 1 fibers. The graphs depict measurements of the movement of a particular spot on the intrafusal fiber in the third lumbrical muscle of a rat hind foot following a 40 micron stretch. Chain fibers rapidly settled to a steady-state position, indicating no mechanical creep to speak of. The bag fiber on the other hand moved back toward the center of the spindle by about a distance of 1 micron over the next roughly 500 msec. The interpretation of this observation is that the SEC was slowly contracting to a shorter length due to "creep". The magnitude of the effect is about 2 to 3% of the length change.

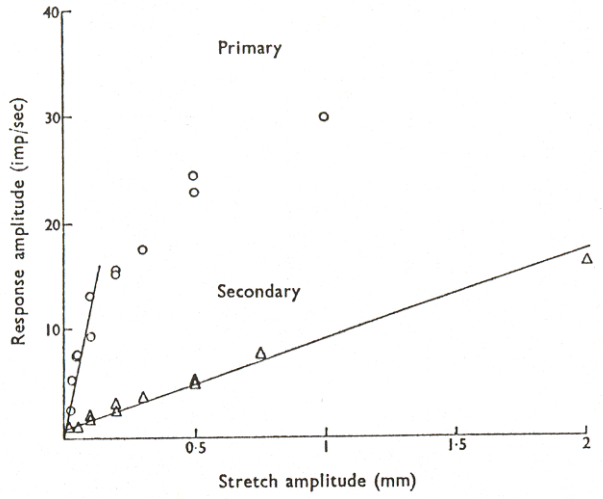

Figure 6: Afferent average firing rate vs. stretch amplitude for primary and secondary afferents. A sinusoidal stretch at a frequency of 1 Hz was applied and average firing rate was measured. The secondary afferent (group II from the chain fiber) showed a linear transfer characteristic. The primary afferent (group Ia) had only a limited linear response region, after which it showed a saturating nonlinearity.

linear transfer characteristic of firing rate vs. amplitude. It is not altogether clear whether the nonlinearity in the primary is due to nonlinearity in the SEC or whether it is due to some property of the sensory neuron itself, or whether both factors are involved. For the units given in figure 6 the shape of the primary response is reasonably well-fitted by

$$y(x) = 21 \cdot \tan^{-1}(6x) \cdot u(x) \quad \text{impulses/sec, } x \text{ in mm.}$$

This suggests that a phenomenological model of this nonlinearity would take the form of an arctangent function of stretch amplitude.

Yet another nonlinearity not accounted for by the Hill model involves an interaction between fusimotor stimulation by gamma motoneurons and what appears to be a kind of sliding friction effect (non-viscoelastic damping in the B element of the model). The effect is called the acceleration response, and it is depicted in Figure 7.[9] If the bag fiber is strongly stimulated by gamma motoneuron firing prior to being stretched, there appears to develop a sharp resistance to stretching in the C+B+PEC section of the Hill model of the intrafusal fiber. This means that the stretch would register almost entirely in the equatorial region of the spindle (i.e. in the SEC) initially, and this is what produces the high firing rate in the initial Ia afferent. After some amount of buildup in T_{SEC} the resistance of the C+B+PEC region suddenly releases (which would allow the SEC to contract) and the firing rate drops. If the gamma motoneuron tetanus is not repeated the effect does not recur. This and other data lead to the hypothesis that an intense and prolonged tetanus applied to a bag fiber produces a static friction effect (which would act in parallel with the viscoelastic damper B). The phenomenon suggests that an intense tetanus leads to some sort of fusing of the actin and myosin filaments in the polar regions of the intrafusal fiber, thus preventing this part of the bag fiber from expanding until some critical tension that depends on the intensity of the stimulus is reached. After this, these "welds" break free and the behavior of the intrafusal fiber returns to normal operation. This static friction effect can persist for many seconds after the tetanus, which is what would be expected if the tetanus produced stable bonds between the actin and myosin filaments in the intrafusal muscle fiber.

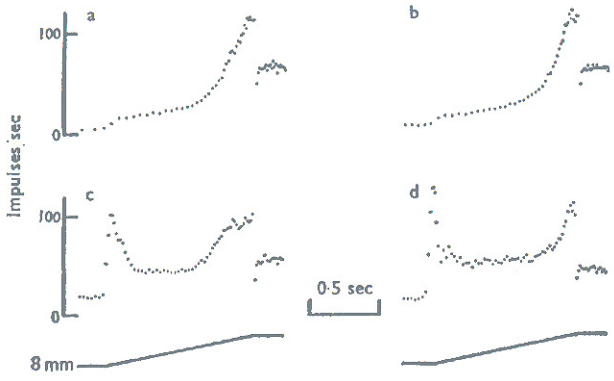

Figure 7: "Acceleration response" of primary spindles following fusimotor stimulation. Figures (a, b) depict normal spindle responses to a ramp stretch. Figures (c, d) illustrate the response of the same primary following a period of repetitive gamma motoneuron stimulation. The ramped stretch was applied 15 seconds after a 1.5 second stimulation at 150 action potentials per second from a dynamic (c) and a static (d) gamma motoneuron efferent. There is a prominent initial burst of Ia afferent firing, followed by a pronounced drop in firing rate to slightly higher than normal levels, and finally a recovery to the normal response. No action potential stimulation was applied during the stretch. If the stretch is repeated without a preliminary AP stimulation the effect does not repeat. This leads to the hypothesis that the initial burst is due to fusimotor-induced friction in the previously activated regions of the intrafusal fiber.

[9] *op. cit.* Matthews, pg. 284, fig. 6.8.

II. The Dynamical Equations of the Linear Model

The dynamical equation for the Hill model in figure 3 is found by equating $T_C + T_B + T_{PEC} = T_{SEC}$ and using the length relationship (1). The result is

$$\dot{x}_p = -\frac{K_{PEC} + K_{SEC}}{B} x_p - \frac{Q_C}{B} + \frac{K_{SEC}}{B} \lambda \qquad (4).$$

It will prove convenient to define the neper frequencies

$$\omega_p \equiv \frac{K_{PEC} + K_{SEC}}{B} \qquad \text{(pole frequency)} \qquad (5a)$$

$$\omega_z \equiv \frac{K_{PEC}}{B} \qquad \text{(zero frequency)} \qquad (5b)$$

and the stiffness ratio

$$\sigma \equiv \frac{K_{PEC}}{K_{SEC}} \qquad (5c).$$

Because intrafusal fibers make no mechanical contribution to limb movement, both the spindle length λ and the fusimotor excitation Q_C are regarded as forcing functions in (4). For several reasons, the most interesting solution to (4) is that for which Q_C is a constant and λ is a ramped step change in length over ramp duration T

$$\lambda(t) = \begin{cases} \lambda_0 + vt, & 0 \le t \le T \\ \lambda_0 + vT, & t > T \end{cases} \qquad (6)$$

where $v \equiv d\ell/dt$. Let the initial fiber lengths be x_{p0} and x_{s0} . These initial conditions are related to the initial length as

$$x_{p0} = \frac{\lambda_0}{1+\sigma}, \quad x_{s0} = \frac{\sigma \lambda_0}{1+\sigma}.$$

We obtain the solutions to (4) under (6) as

$$\begin{aligned} x_p(t) = {} & \frac{\lambda_0}{1+\sigma} - \frac{Q_C}{K_{PEC} + K_{SEC}} \left(1 - e^{-\omega_p t}\right) \\ & + \frac{vt}{1+\sigma} - \frac{v \cdot (t-T)}{1+\sigma} \cdot u(t-T) \\ & - \frac{v\tau_p}{1+\sigma} \left(1 - e^{-\omega_p t}\right) + \frac{v\tau_p}{1+\sigma} \left(1 - e^{-\omega_p (t-T)}\right) \cdot u(t-T) \end{aligned} \qquad (7a)$$

and

$$x_s(t) = \frac{\sigma\lambda_0}{1+\sigma} + \frac{Q_C}{K_{PEC}+K_{SEC}}\left(1-e^{-\omega_p t}\right) + \frac{\sigma\cdot v t}{1+\sigma} - \frac{\sigma\cdot v\cdot(t-T)}{1+\sigma}\cdot u(t-T) + \frac{v\tau_p}{1+\sigma}\left(1-e^{-\omega_p t}\right) - \frac{v\tau_p}{1+\sigma}\left(1-e^{-\omega_p (t-T)}\right)\cdot u(t-T) \quad (7b)$$

where $\tau_p \equiv 1/\omega_p$ and *u* is the unit step function.

In the steady state (as *t* goes to infinity), the solutions of equations (7) approach

$$\lim_{t\to\infty} x_p(t) \equiv x_{p\infty} = \frac{\lambda_0 + vT}{1+\sigma} - \frac{Q_C}{K_{PEC}+K_{SEC}}$$
$$\lim_{t\to\infty} x_s(t) \equiv x_{s\infty} = \frac{\sigma}{1+\sigma}(\lambda_0 + vT) + \frac{Q_C}{K_{PEC}+K_{SEC}} \quad (7c).$$

The peak values of the responses occur at *t* = T and are given by

$$x_p(T) = \frac{\lambda_0}{1+\sigma} - \frac{Q_C}{K_{PEC}+K_{SEC}}\left(1-e^{-\omega_p T}\right) + \frac{vT}{1+\sigma} - \frac{v\tau_p}{1+\sigma}\left(1-e^{-\omega_p T}\right) \quad (7d)$$

$$x_s(T) = \frac{\sigma\lambda_0}{1+\sigma} + \frac{Q_C}{K_{PEC}+K_{SEC}}\left(1-e^{-\omega_p T}\right) + \frac{\sigma\cdot vT}{1+\sigma} + \frac{v\tau_p}{1+\sigma}\left(1-e^{-\omega_p T}\right) \quad (7e).$$

These solution all assume the *x* terms exceed the slack lengths of the elastic elements. It is also worth noting that

$$\frac{Q_C}{K_{PEC}+K_{SEC}} = \frac{Q_C/K_{SEC}}{1+\sigma} \quad (8).$$

The response of the system to sinusoidal excitation is also of interest, so long as the intrafusal fiber remains within the linear region of operation. Here the analysis is made somewhat difficult by the fact that the system has two forcing function inputs. If we assume a sinusoidal stretch of peak amplitude Λ is applied and that Q_C is proportional to this as $Q_C = h\Lambda$, where *h* is possibly a complex number (to denote a phase difference between fusimotor excitation and the sinusoidal stretch), then letting *s* denote the Laplace transform complex frequency variable (4) transforms in the sinusoidal steady state as

$$X_s(s) = \left(\frac{h/B}{s+\omega_p} + \frac{s+\omega_z}{s+\omega_p}\right)\Lambda \quad (9).$$

From equations (5) we note that $\omega_z < \omega_p$, so when $h = 0$, (9) is the transfer function of what in control system terms is known as a "lead network".

In the more general case where we make no assumptions of a relationship between Q_C and the fiber length, the Laplace transform expression for x_s after the transient from the initial condition has died out is given by

$$X_s(s) = \frac{Q_C(s)}{s+\omega_p} + \frac{s+\omega_z}{s+\omega_p}\Lambda(s) \qquad (10).$$

In order to experimentally confirm this model, it would be best to try to get a direct measurement of fiber movement under conditions where the two input signals are controlled. Unfortunately, such an experimental arrangement seems to be quite difficult to make. As an alternative, one could try to relate sensory firing rates vs. sinusoidal stretches as a function of frequency. It is widely held that the responses of group II spindle afferents (secondary afferents) is more or less directly related to stretch length (figure 6), and so examination of group II firing rate as a function of stretch frequency should give us data about the soundness of (10) as well as of the relative values for the parameters of the mechanical model.

An experiment of this sort was reported in a landmark paper by Matthews and Stein.[10] Their experiment leaves a bit to be desired insofar as confirming or refuting the Hill model is concerned, but Matthews and Stein were investigating primary and secondary spindle afferent firing characteristics rather than attempting a model validation. There are a couple of caveats we must be aware of in trying to interpret their results in terms of the consequences of these results for (10). The experiment was performed on live, decerebrate cats. The "appropriate" dorsal roots were cut, thereby breaking the direct feedback from the muscle to the spinal cord, but the ventral root was left intact. This means that Q_C is not zero in (10) and, unfortunately for us, they did not measure the "spontaneous" fusimotor firing activity of the gamma motoneurons. Therefore Q_C in their experiment is unknown. However, it is reasonable to suppose that to at least a first approximation Q_C is uncorrelated to $\lambda(t)$ in the experiment. It will therefore contribute a "noise floor" to Matthew's and Stein's measurements of $|X_s|$, and this noise floor will not necessarily be constant (Q_C might and probably will be "colored" noise). For typical spontaneous firing patterns of gamma motoneurons, the noise corruption should be worst at low frequencies and less important at higher frequencies. My examination of their results leads me to believe that the noise term is negligible above frequencies of 0.3 Hz in their experimental results but that it is substantial at frequencies lower than this.

The second caveat is that Matthew's and Stein's method of measuring the spindle firing rate to obtain a transfer function characteristic is an inherently noisy process, particularly where the measurement of phase is concerned. They employed what I would regard as a sound method in determining the firing rate vs. time and relating this to the stretch amplitude, but they provided no data on the variances of the measurements. It is therefore difficult to tell when discrepancies between a model and the measured results are significant and when they are not. Figure 8, taken from their paper, illustrates the noise in their measurement process. This noise will have a much more serious corrupting effect on their estimates of phase than on their estimates of magnitude, although its effect on magnitude estimation is by no means negligible either. I estimate the signal to noise ratio for this measurement as about 2.5 to 3.8 dB, which translates in their experiment to a phase noise standard deviation on the order of 11° to 16° at low frequencies. The measured phase error as frequencies increase will <u>not</u> be zero-mean but rather will be biased a few degrees to the negative.

[10] P.B.C. Matthews and R.B. Stein, "The sensitivity of muscle spindle afferents to small sinusoidal changes of length", *J. Physiol.* (1969), **200:** 723-743.

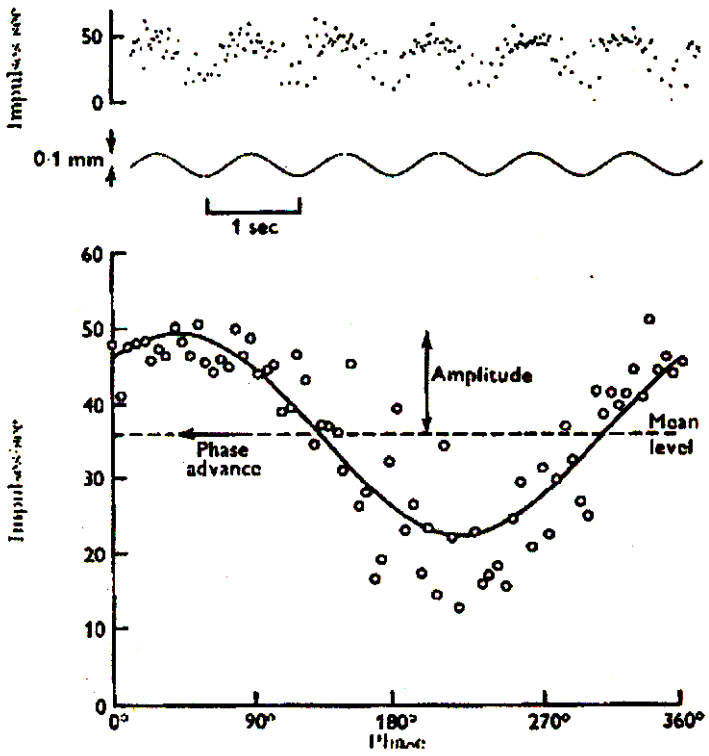

Figure 8: Typical Matthews-Stein measurement of firing rate response. The top graph is firing rate in impulses per second vs. time. The middle graph is the mechanical stretch being applied. The bottom graph displays their measured data (impulses per second vs. phase angle in one cycle of the sinusoid) and a least-squares curve fit of a general sinusoid to this data.

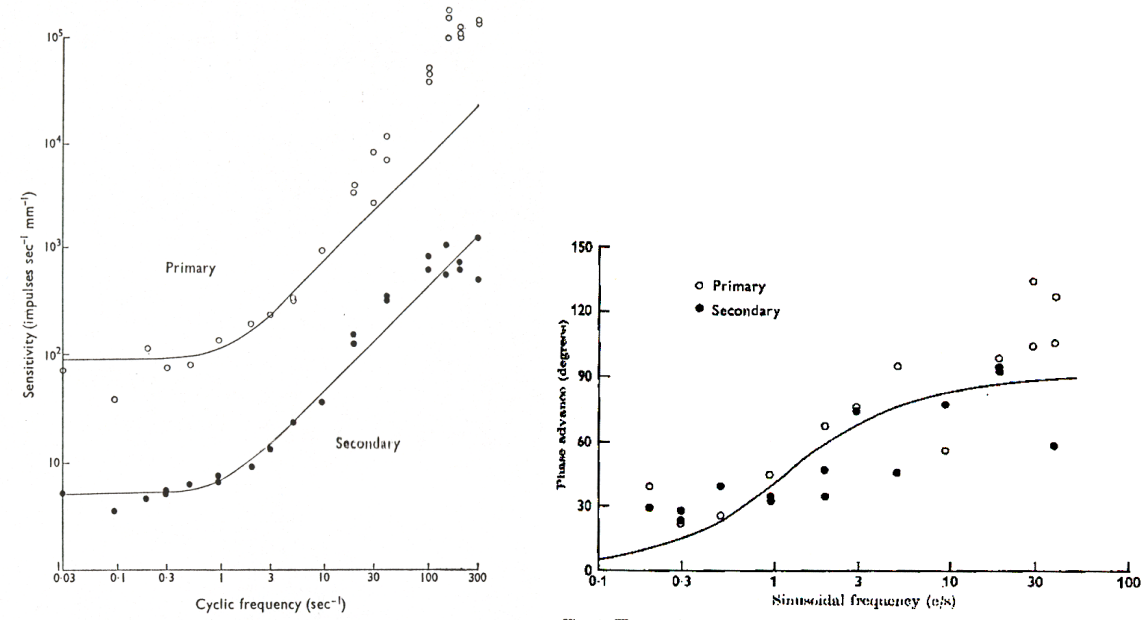

a b

Figure 9: Firing rate per mm transfer functions from Matthews and Stein. (a) is the magnitude response; (b) is the phase response. Solid lines are theoretical curves given in their paper.

Matthews and Stein assumed a rather simple model for their firing rate behavior. In effect, they used

$$H(s) = S \cdot (1 + s/\omega_z)$$

where S is a scaling factor and ω_z corresponds to (5b). They found reasonably good agreement between this model and the response of the secondary spindle in the range from 0.3 Hz to 20 Hz. Because they were not considering the Hill model, they paid little attention to the response of their curves above 100 Hz, where it is clear that their data is departing "flatline" from their model curve in the magnitude response. I have analyzed their data with respect to (10) and I find that the data is not statistically inconsistent with (10) when $\omega_z = 2\pi \cdot 1.4$ and $\omega_p = 2\pi \cdot 104$ rad/sec. These numbers provide reasonable agreement with both the magnitude and the phase plots in figure 9. These values imply that the stiffness ratio (5c) is $\sigma = 0.014$.

It may seem odd indeed that the SEC should be some 70-times more stiff than the PEC, but this experimental data does so indicate. This would be consistent with the sensory area of the intrafusal fiber being so much shorter in length than the contractile area. On the other hand, there are other fairly strong arguments (arguments, not proofs) that favor the idea that the SEC should be less stiff (more elastic) than the contractile region of the fiber's poles.[11] If in fact that were true, then the Matthews & Stein data would flatly contradict the Hill model *if* it is also true that secondary afferents respond in direct proportion to stretch or contraction length (as does seem to be largely the case). This is because if $K_{SEC} < K_{PEC}$ then $\sigma > 1$ and the +20 dB per decade slope exhibited in figure 9(a) could not rise for two decades in frequency, nor could the high frequency sensitivity be so much greater than the low frequency sensitivity.

Another apparent contradiction between figure 9(a) and other experimental results comes from the relatively high pole frequency, ω_p. The value of 104 Hz that I deduced from the Matthews and Stein data implies a time constant of about 1.5 msec. This value seems to be greatly at odds with other experiments measuring the speed of contraction of intrafusal fibers. Figure 10 is taken from a paper by Smith.[12] The figure demonstrates that chain fibers can change lengths more quickly than bag fibers (by about a factor of 2) when stimulated by 2 msec pulses coming at 20 msec intervals (50 pulses per second). The problem is in the time constant suggested by these responses. The curves go approximately in the shape of a $1 - \exp(t/\tau)$ function that would indicate values for ω_p of about 12 rad/sec (1.9 Hz) for the chain fiber and about 5 rad/sec (0.8 Hz) for the bag fiber. These are values far closer to the value for ω_z in figures 9 than for ω_p. On the other hand, we must keep in mind that the responses shown in figure 10 must also take in the dynamical equation for $Q_C(t)$ and do not represent a purely mechanical set of dynamics. Stimulation was not applied via motoneurons but rather via an experimental setup where the electrical signal was applied across a Vaseline seal. Therefore, the time course for $Q_C(t)$ is completely unknown. The situation is sufficiently confounded by multiple factors so as to not serve to convincingly refute the Hill model, but the time domain discrepancy is nonetheless quite disturbing. It should be noted that the conditions under which figure 10 was obtained involve movements much larger than those of the Matthews-Stein experiment, and this might introduce a

[11] *op. cit.* Matthews pp. 279-282.
[12] R. Smith, "Properties of intrafusal fibers," in *Proc. 1st Nobel Symposium: Muscular Afferents and Motor Control*, NY: John Wiley, 1966, pp. 69-80.

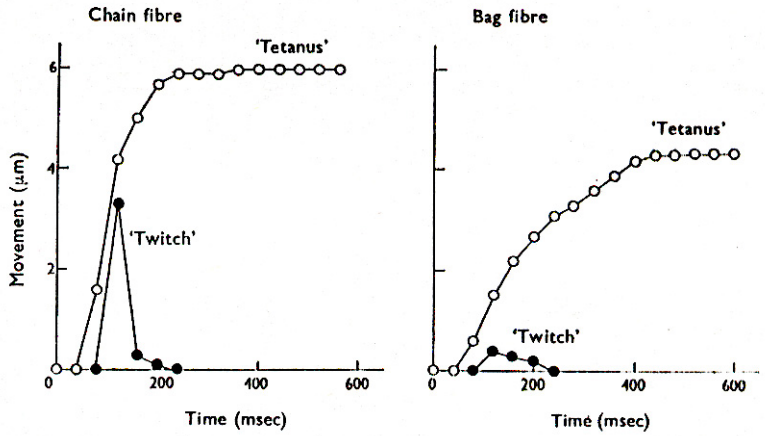

Figure 10: Movement response of chain and bag fibers to electrical stimulation. The shape of the tetanus response roughly follows a $1 - \exp(t/\tau)$ function corresponding to a pole frequency of about 12 rad/sec for the chain fiber and about 5 rad/sec for the bag fiber. The data was obtained from a partially isolated spindle containing a few intrafusal fibers from the third lumbrical muscle of the rat hind foot at 20-23° C. Stimulation was by 2 msec electrical pulses applied to the spindle across a Vaseline seal. $Q_C(t)$ would therefore not reflect *in vivo* conditions.

a nonlinearity in the response that would not show up in experiments that measure secondary afferent firing rate data such as shown in figure 6. If K_{SEC} or K_{PEC} were to decrease as the length of the movement increased, this would have the effect of reducing ω_p, thus increasing the time constant.

Because the intrafusal fibers are not involved directly in the generation of movement, but only in the instrumentation of movement to produce sensory feedback, resolving these questions pertaining to the mechanical properties of intrafusal fibers is less important for our purposes than accurately modeling the afferent response to limb movement. For this task, the experimental data in figures 9 is the most relevant, and we do have a Hill model that seems to adequately fit this purpose. There is, however, another caveat that attaches to figure 9. Matthews and Stein did not undertake to identify what type of intrafusal fibers were associated with their afferent data. Because chain fibers tend to predominate in the generating of group II afferent signals, it is probably a safe bet to assume that the model parameters given above are those of chain fibers.

The parametric data for bag fibers, whether bag 1 or bag 2, is not so clearly illuminated by the data in figures 9 because the response for the primary afferents departs significantly from what would be expected solely on the basis of the Hill model. Between about 5 Hz and 100 Hz, the primary response exhibits a slope of about 30 dB per decade, which is a very strange slope and not one producible by a lumped parameter model. Such a slope is indicative of a response that rises as the 3/2 power of frequency. Whether this is due to some nonlinearity of bag fibers or is due to some property of group Ia sensory neurons is not known. At around 100 Hz the slope breaks again, dropping to 10 dB/decade (a ½ power of frequency). This would be consistent with the 100 Hz high frequency pole seen for the chain fiber. Moreover, figure 9(a) has a low frequency data point that might possibly indicate the presence of an additional dynamic taking the form of an additional differentiation with an accompanying transfer function pole at a frequency of about 0.3 Hz (1.9 rad/sec or a time constant of about 530 msec.). Matthews and Stein noted this feature of their data but stated that because their measurements were so unreliable in this frequency range they could not draw any firm conclusions about it, including whether or not the effect was real or due to experimental error.

This gives us the rather unexpected result that the primary and secondary curves, insofar as they are influenced by the mechanical factors of the Hill model, exhibit the same pole and zero frequencies. This is very surprising if indeed the secondary ending data comes from chain fibers rather than bag fibers. It would imply that the stiffness to damping factor ratio is the same for both types of fibers. If this is true, it implies that any differences between primary and secondary afferent signals is due only to differences in the dynamics of fusimotor excitation, $Q_C(t)$ and differences between type Ia and type II sensory neurons.

In part I of this tech brief I suggested the use of a 10 msec sampling interval Δt in modeling the extrafusal muscle fibers. Here we see that the time constant for the intrafusal Hill model is much faster, on the order of 1.5 msec. The use of step-invariant discretization at a 10 msec sampling interval is therefore inappropriate. What is proposed instead is that a ramp invariant discretization, corresponding to a first-order hold approximation, be used. The velocity term in the solutions to the dynamical equations given above is estimated at time t as

$$v(t) = \frac{\ell(t) - \ell(t - \Delta t)}{\Delta t} \tag{11}$$

where ℓ is the muscle length. The duration of the ramp is taken as $T = \Delta t$.

III. Spindle Afferent Properties

The spindle sensory neurons are the transducers of muscle state. They fall into two classes, type Ia (which produces our group Ia spindle afferents) and type II (which produces our group II spindle afferents). These sensory neurons differ from the neurons we have discussed in earlier tech briefs in several ways. First, they have no dendrites. The sensory element is a nerve ending in the muscle tissue at one end of a long axon. This axon travels to the cell body, located in the dorsal root ganglia, and continues on through the dorsal root to the spinal column.

It would be simpler for us if the sensory nerves followed a "one fiber, one nerve" rule but, alas, they do not. Figure 11 illustrates the arrangement of sensory nerve endings on the intrafusal muscle fibers. The primary (group Ia) ending splits off into multiple spiral endings that attach to

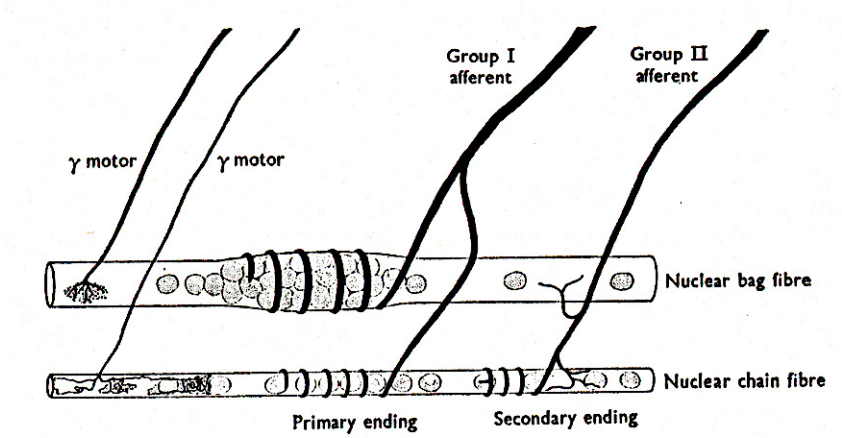

Figure 11: Sensory nerve endings in muscle spindles. Observe the branching that takes place and that each afferent attaches to multiple intrafusal fibers.

every fiber in the spindle (bag 1, bag 2, and all the chain fibers). The diameters of these spiral endings vary, depending on the type of fiber it is attached to, but the spiral pitch appears to be about the same in every case. The resemblance of this arrangement to an axial helical spring is rather obvious, which raises the question of to what extent the nerve ending contributes to the stiffness of the receptor region (i.e. to the stiffness of the SEC). I don't have an answer for this, but it is interesting to note that for a long spring (which, judging from figure 1, is an approximation that might apply to this case) the stiffness of an axial helical spring is proportional to the 4th power of the diameter of the turns, inversely proportional to the number of turns, and inversely proportional to the 3rd power of the radius of the turns. If the scale depicted here or in figure 2 is representative, this would tend to suggest a lower stiffness for bag fibers than for chain fibers so far as K_{SEC} is concerned. This is enough to make one wonder if the data in figure 9(a) for the primary endings might not be dominated by chain fibers since the frequencies for the zero and the pole in the response were the same as for the secondary afferents data. Of course, this assumes that the contribution to stiffness by the nerve windings is at all significant, which is by no means established so far as I know. The diameter of the nerve is on the order of a few microns, much smaller than the spiral radius, and stiffness goes by the 4th power of this diameter. Thus it would not be surprising if, and even seems to me likely that, these "nerve springs" contribute nothing at all to K_{SEC}.

In the case of the group II afferents, I'm afraid that I've been confronted with contradictory statements as to its nature. Pearson and Gordon claim that the secondary afferent wraps around every bag 2 ("static") and every chain fiber in the spindle, and does so in all cases in the form of a spiral.[13] Matthews[14] and others dispute this claim, saying that while the group II fiber does spiral around every chain fiber in the spindle, it only occasionally (and sometimes never) involves the bag 2 fiber. When it does involve the bag 2, they claim it does not do so as a spiral but rather as a "spray" (as depicted in figure 11). Both camps agree that group II nerves do not involve bag 1 fibers. The article by Pearson and Gordon is the most recent, and is based on a 1980 work by Boyd, but it is not clear to me whether their claims regarding the group II nerve is actually based on Boyd's review or represents a misinterpretation of the article. (Pearson's and Gordon's article is not primarily about muscle spindles). The claims of the other group also reference Boyd's work but do so from earlier of his papers and from other authors' articles. Therefore, until I get a chance to read the 1980 Boyd review, my inclination is to go with the arrangement as depicted by figure 11, and to the long-held findings that group II afferents principally involve chain fibers.

The behaviors of the primary and secondary afferents in response to simulation are markedly different. Furthermore, their responses to muscle motion also depends on the state of intrafusal muscle fiber stimulation by their gamma motoneurons. The effect of motoneuron excitation is more complex for primary than for secondary afferents. Figure 12[15] is an illustration of the primary and secondary afferent responses to mechanical stimulation in the absence of gamma motoneuron activity.

We first examine the response of the primary afferent. For the linear stretch (increasing λ), there is an increase in firing rate during the ramp. Note that during the initial stages of the ramp this firing rate is relatively constant, which indicates that the primary's firing rate is proportional to the *slope* of the ramp. This characteristic is how the primary afferent came to be regarded as a velocity sensor. However, near the end of the ramp (in this example) we can note a small increase

[13] K. Pearson and J. Gordon, "Spinal reflexes", in *Principles of Neural Science*, 4th ed., E. Kandel et al. (eds.), NY: McGraw Hill, 2000.
[14] *op. cit.* Matthews, pg. 31.
[15] *op. cit.* Matthews, pg. 157.

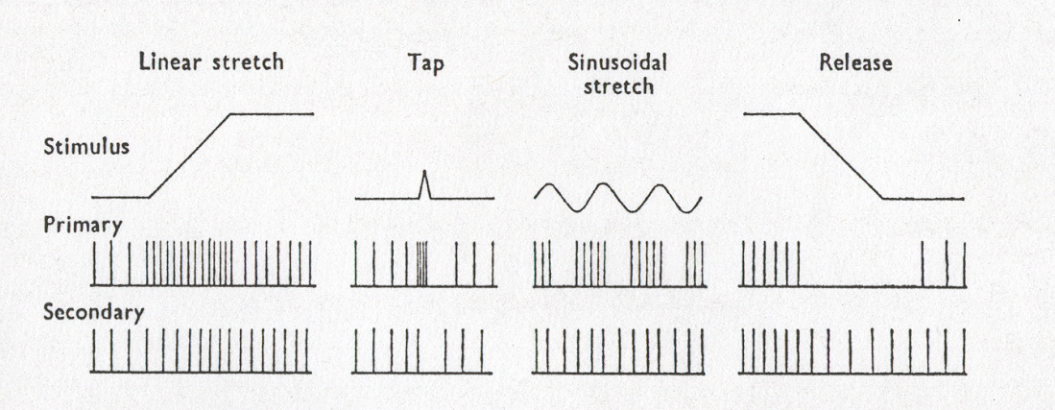

Figure 12: Typical responses of primary and secondary afferents to large stretches in the absence of fusimotor activity. Responses are shown for the cases of a linear ramped stretch (increasing muscle length), a "tap" simulating a muscle twitch, sinusoidal stretching, and a ramped decrease in muscle length resulting from the release of a muscle that had been stretched beyond its normal resting length. See text for discussion.

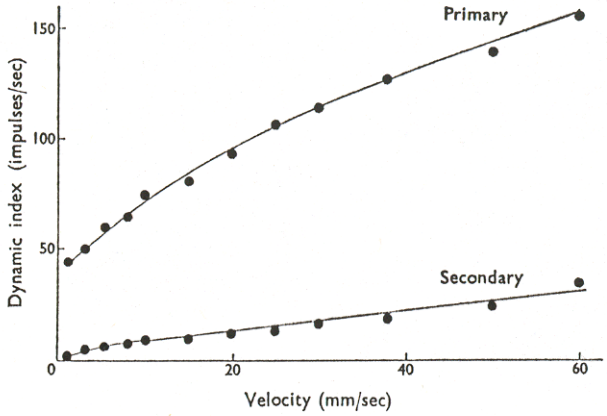

Figure 13: Dynamic index for primary and secondary afferents. The dynamic index is the difference, in impulses per second, between the peak firing rate during a ramp and the average firing rate after the end of the ramp. The curves here give the dynamic indices in the absence of fusimotor activity (i.e. in the absence of firing by gamma motoneurons).

in the primary's firing rate. This is interpreted by saying that the Ia afferent signal also carries some position information in addition to the velocity information. At the end of the ramp there is a small break in primary firing, followed by resumed firing at a rate higher than before the stretch but lower than the firing rate during the stretch. The difference between the peak firing rate during the ramp and the average firing rate after the ramp is known as the *dynamic index*, which is an important metric in characterizing spindle afferents. As might be expected, the dynamic index for primary afferents is a strong function of the ramp velocity. Figure 13 illustrates typical dynamic indices for primary and for secondary afferents in the absence of fusimotor activity.[16] As shown in the figure, the secondary also exhibits a dynamic index, although not nearly so much as does the primary. This difference between peak and steady-state post-ramp firing rate is barely discernible in figure 12 for the secondary.

[16] *op. cit.*, Matthews, pg. 151.

The tap response of the primary is interesting. It exhibits a high rate burst of firing, corresponding to the steep slope of the tap, until the peak stimulus is reached. As the tap stimulus peaks and begins to fall, the primary ceases to fire any pulses at all for a short time. It then resumes firing at the rate it exhibited prior to the stimulus. This break in firing seems to be a consistent characteristic of primary afferents in the absence of fusimotor activity. We can see this quite vividly in the primary's response in the release case (where the muscle is shortening rather than stretching). Turning finally to the sinusoidal stimulus response, we see a more or less constant firing rate by the primary during the upswing of the sinusoid (when the velocity is positive) and the characteristic break in firing during the downward swing (when the velocity is negative). Firing resumes at the minima of the stimulus and ceases at the maxima. We may note that the constant firing rate depicted in figure 12 is note entirely constant, showing a maximum in firing rate as the sinusoid crosses zero (where its slope, and therefore the velocity of the stimulus) is greatest.

Next we turn to the secondary afferent. We have already remarked on its ramp response. The secondary shows an advance in the firing of its pulse that occurs during the tap, and appears to exhibit a brief break in firing during recovery of the tap. Is this break similar to that shown by the primary? The other three stimulus cases indicate that it is not. During the sinusoidal stimulus the secondary firing rate more or less follows the amplitude of the stimulus, increases during the up-swing, decreasing during the downswing, and reaching the largest inter-pulse interval at the minima, the smallest at the maxima of the stimulus. Its response for the release case is interesting. The secondary maintains its firing during the downward-going ramp, but note that this firing rate is actually slower than the steady-state firing rate after the end of the ramp down. In fact, the explanation for this is simple and it reflects the dynamical behavior of x_s and x_p during the ramp. Because of the damper in the Hill model, the PEC cannot change its length instantaneously, and therefore changes in total length tend to be transmitted directly to the SEC (where the sensor is located). Only afterwards does the PEC's length change begin to "catch up" and the SEC readjusts until the two springs balance out. This is, in fact, the principal origin of the dynamic index characteristics of the spindle afferents.

In the absence of fusimotor activity, to a first approximation we can say that the primary afferent is a velocity sensor with a small amount of position information added in, while the secondary afferent simply signals muscle length. These differences in operational character can become much less pronounced during firing by static gamma motoneurons, or they can be enhanced during firing by dynamic gamma motoneurons. Fusimotor activity also has a pronounced effect on firing rates for both primary and secondary afferents. This is illustrated in Figure 14.[17] The data here was taken from the decerebrate cat with ventral roots intact and after the ventral roots were cut. The graphs measure firing rate as a function of muscle extension.

The first thing we may note is that fusimotor activity (the firing of gamma motoneurons) substantially increases the sensitivity of both primary and secondary afferents. We may also note that fusimotor activity results in a baseline "pacemaker-like" firing of the spindle afferents at zero extension, whereas in the absence of fusimotor activity both the primary and the secondary cease fire below some minimum muscle length. (We say the intrafusal fibers have gone slack). Above this "slack length", the firing rate vs. extension curves are more or less linear. There is no velocity effect in the primary in this graph because the firing rates were measured at zero velocity. It is worth comparing the primary response in figure 14 with the firing rate response under sinusoidal excitation in figure 6. The nonlinearity evident in figure 6 is absent in figure 14. To me this seems

[17] *op. cit.* Matthews, pg. 154.

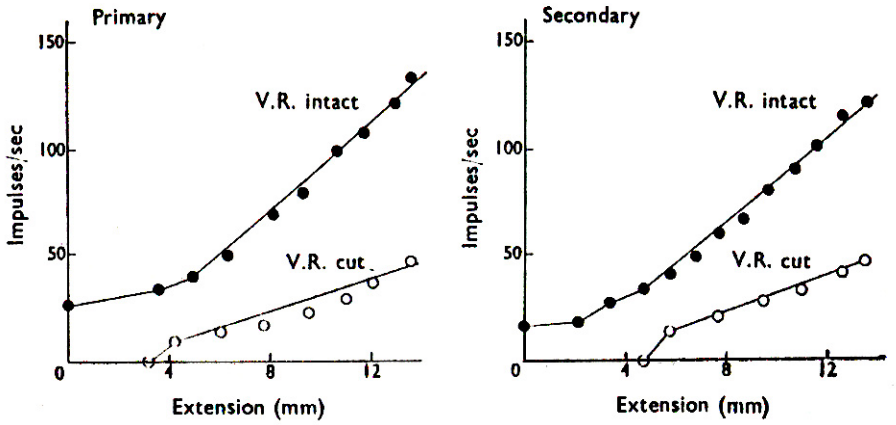

Figure 14: Firing rates vs. extension length of spindle afferents. V.R. intact denotes that the ventral roots were intact and gamma motoneuron excitation of the spindle was present. V.R. cut denotes that the ventral roots were cut and therefore no fusimotor activity was presented to the spindle. The firing rate data was measured 0.5 sec after the application of each stretch.

to indicate that the nonlinear effect reported on in figure 6 must involve the velocity dependence of the primary afferent response rather than its length dependency. It is unclear whether the root cause of this effect is due to nonlinearity in the damper in the Hill model (e.g. that the damper follows the Hill equation discussed in part I), or whether it is due to some property of the Ia nerve ending itself.

The nuclear chain fiber is innervated only by static gamma motoneurons and dynamic beta motoneurons. So far as gamma motoneuron excitation of chain fibers is concerned, there is nothing more of particular interest to say about the relationship between fusimotor activity and secondary spindle response. (There is something interesting to say about it when it comes to characterizing the parameters of $Q_C(t)$, but we will see this later). This is not the case where bag fibers are concerned.

Recall that there are two distinct types of bag fibers. Bag 1 fibers are innervated by dynamic gamma motoneurons. Bag 2 fibers are innervated by static gamma motoneurons. Both are innervated by both types of beta motoneurons. The Ia afferent response is affected differently by these two types of gamma motoneuron activity. This is illustrated in Figure 15 below.[18] Figure 15(a) illustrates the instantaneous Ia firing rate for (1) no fusimotor stimulation; (2) stimulation of the static gamma motoneuron at 70 APs/sec; and (3) stimulation of the dynamic gamma motoneuron at 70 APs/sec. The mechanical stimulus was a 6 mm ramp applied at 30 mm/sec ramp velocity. Figure 15(b) illustrates the time domain response for these same three cases.

In the absence of fusimotor stimulation there was no firing prior to the onset of the ramp. At the onset of the ramp firing begins abruptly, jumping to a rate of about 70-80 impulses per second. This firing is maintained at a constant rate until the ramp reaches an extension of about 3 mm, at which time the firing rate jumps again to a level of about 110-120 impulses/sec. Note from figure 14 that the 3 mm extension corresponds to the slack point in the primary firing rate when the ventral root is cut. At the end of the ramp the firing rate drops to a level consistent with the curve in figure 14.

Stimulation of the static gamma motoneuron affects the bag 2 fiber. MN activity in the graph

[18] *op. cit.*, Matthews, pp. 205-206

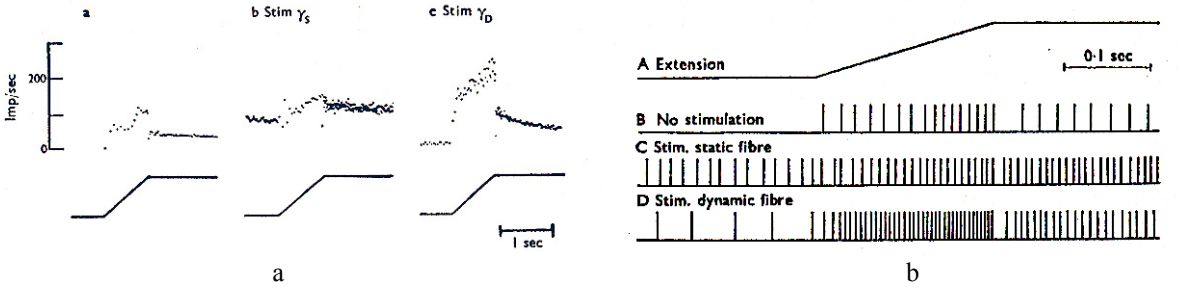

Figure 15: Effect of fusimotor stimulation on primary afferent response. (a) plots the instantaneous firing rates (impulses per sec) during a 6mm stretch at 30 mm/sec in the absence of fusimotor stimulation, with stimulation of the static gamma motoneuron at 70 APs/sec, and with stimulation of the dynamic gamma motoneuron at 70 AP/sec. (b) shows the time domain firing response under these same conditions. The scale for instantaneous firing rate is 100 impulses per division.

was initiated prior to the beginning of the ramp. Fusimotor stimulation of bag 2 produced a background firing rate of about 100 impulses/sec prior to the onset of the ramp. When the ramp was applied firing rate increased in proportion to the extension after a brief transient at the beginning of the ramp. This response is rather like what one would expect from a secondary afferent, i.e. it follows muscle length rather than velocity. At the end of the ramp there was a brief break in firing, followed by resumption of firing at a slightly lower level (small dynamic index). The steady-state firing rate is higher than would be expected from figure 14 at an extension of 6 mm, possibly indicating that fusimotor stimulation at 70 APs/sec exceeds the spontaneous background fusimotor activity under the conditions at which figure 14 was measured.

Stimulation of the bag 1 fiber (in the absence of bag 2 fusimotor stimulation) produces a quite different response. Background firing is again produced, but at a significantly lower firing rate than was produced by bag 2 stimulation. At the onset of the ramp there is a sudden jump to a higher firing rate, followed by continued increasing of the instantaneous firing rate that more or less follows the mechanical extension. At the end of the ramp there is a short break in Ia firing, followed by resumption of firing at a lower and gradually decreasing rate. The dynamic index of firing is much greater in this case than for stimulation of the static gamma motoneuron.

These results illustrate the principal difference between static and dynamic fusimotor activity in the primary response. Dynamic stimulation increases the normal dynamic responsiveness of the primary ending, static fusimotor activity decreases the dynamic responsiveness. Here dynamic responsiveness is judged in terms of the dynamic index. Figure 16 illustrates this effect more clearly by plotting the dynamic index for different levels of fusimotor stimulation as a function of ramp velocity.[19] For stimulation of static gamma motoneurons there is a general decrease in the dynamic index, this becoming less responsive to further increases in fusimotor firing rate as the firing rate increases. The dynamic index vs. velocity curves are approximately linear.

Stimulation by dynamic gamma motoneurons produces an increase in dynamic index. The dynamic index vs. velocity curve becomes more pronouncedly curved as fusimotor firing rate increases. Because the dynamic index is a kind of measure of how much velocity contributes to Ia firing rate, we can view these results as indicating that dynamic fusimotor activity tends to make the primary more of a velocity sensor, static fusimotor activity tends to make it more of a position

[19] *op. cit.*, Matthews, pg. 207.

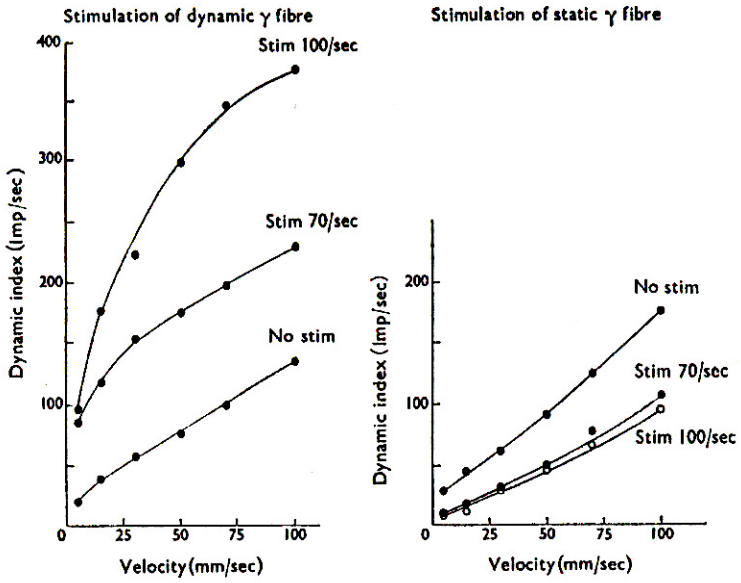

Figure 16: Dynamic index of primary endings vs. velocity at different levels of fusimotor activity. Dynamic and static gamma motoneurons were excited one at a time. The firing rate 0.5 sec after the end of the ramp is subtracted from the peak instantaneous firing rate, which occurs at the end of the ramp, to obtain the dynamic index. Dynamic fusimotor activity increases the dynamic index, static fusimotor activity decreases it. Results given here are for a stretch of 6 mm.

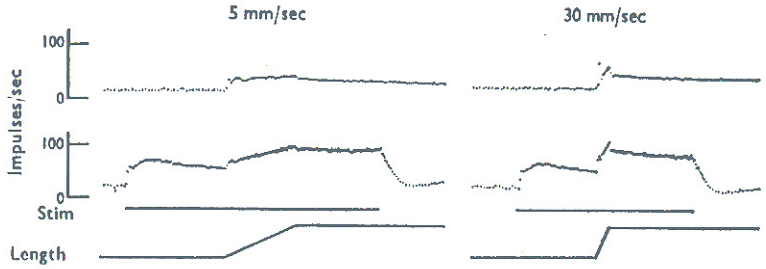

Figure 17: Effect of static fusimotor activity on secondary afferent. Top traces are taken with no fusimotor activity. The bottom traces are for static fusimotor stimulation at 100 APs/sec. Stretch velocities were 5 mm/sec (left side) and 30 mm/sec (right side). Total extension was 5 mm.

sensor. Because dynamic gamma motoneurons innervate bag 1 fibers but not bag 2 fibers, this evidence suggests that the primary ending on the bag 1 fiber is the transducer for velocity information, while the primary ending on the bag 2 fiber is the transducer for muscle length (so far as this information is carried by Ia afferents).

Bag 1 fibers carry no secondary afferent endings and dynamic gamma motoneurons do not innervate bag 2 or chain fibers. Therefore, it is to be expected that dynamic fusimotor activity has no effect on the secondary afferent. On the other hand, some bag 2 fibers do carry secondary endings and some static gamma motoneurons innervate both a bag 2 and a chain fiber (see "Muscles" tech brief, figure 6). Therefore we can expect static fusimotor activity to have some effect on the secondary afferent. This is illustrated in Figure 17.[20] What we find is that static fusimotor activity increases the sensitivity of the secondary afferent to position sensing but does

[20] *op. cit.*, Matthews, pg. 210.

not affect the dynamic index. This reconfirms the role of the secondary afferent as a pure length sensor without any appreciable velocity component in its signal.

Static fusimotor activity has another effect on the primary response that is noteworthy. We have seen already that the primary afferent demonstrates a pause in its firing during the downward swing of muscle length. What causes this pause in firing? Figure 18 illustrates the primary response to sinusoidal stretching under dynamic and under static fusimotor excitation.[21] What is most noteworthy in this figure is that under sufficiently strong static fusimotor stimulation the break in firing rate could be eliminated and the primary made to better follow the instantaneous value of the muscle length. Stimulation of the dynamic gamma motoneuron did not eliminate the break in firing under the conditions where this data was taken.

Recalling that the bag 1 and bag 2 sensory endings merge with each other at the main root of the sensory neuron's axon, one plausible interpretation for these results is as follows. Negative velocities may cause the sensory ending on the bag 1 fiber to become hyperpolarized. This membrane potential spreads electrotonically to the junction with the nerve ending coming from the bag 2 fiber. If the hyperpolarization from the bag 1 ending is able to overcome the depolarization coming from the bag 2 ending, no action potentials are generated in the threshold region of the primary axon. On the other hand, if the static fusimotor excitation is high enough so that the bag 2 signal is stronger than the velocity signal from bag 1, then the firing threshold can still be exceeded in the primary main axon and no break in firing is registered.

The amplitude and frequency of the mechanical stimulus exceeds the linear range of primary operation under the conditions of the test leading to figure 18. Additional interesting effects come to light when the amplitude of the mechanical stimulus does not exceed the linear range of the primary except when the fibers are not contracting. This is illustrated in Figure 19.[22] In this figure, the amplitude of the mechanical stimulus was reduced to 0.1 mm peak-to-peak. The intrafusal fibers were still operating within the linear range when fusimotor stimulus was applied, but the mechanical stimulus exceeded the linear range during the upswing (positive velocities).

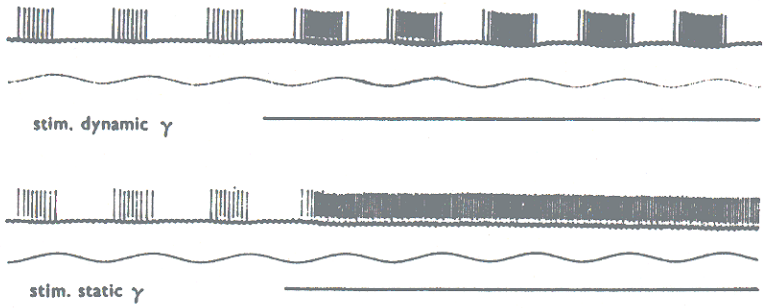

Figure 18: Effect of static fusimotor stimulation on sinusoidal response of the primary. The peak-to-peak amplitude of the stretch was 1 mm and the frequency was 3 Hz. Fusimotor stimulation at 100 APs/sec was applied during the time interval indicated by the solid underbars in the figure. Dynamic fusimotor stimulation increased the rate of firing of the primary but did not affect the break in firing during negative velocities. Static fusimotor stimulation also increased the firing rate, but at the level of stimulus shown here eliminated the break in firing rate. The firing rate under static fusimotor stimulation was better able to follow the instantaneous amplitude of the mechanical stimulus.

[21] *op. cit.*, Matthews, pg. 213.
[22] *op. cit.*, Matthews, pg. 214.

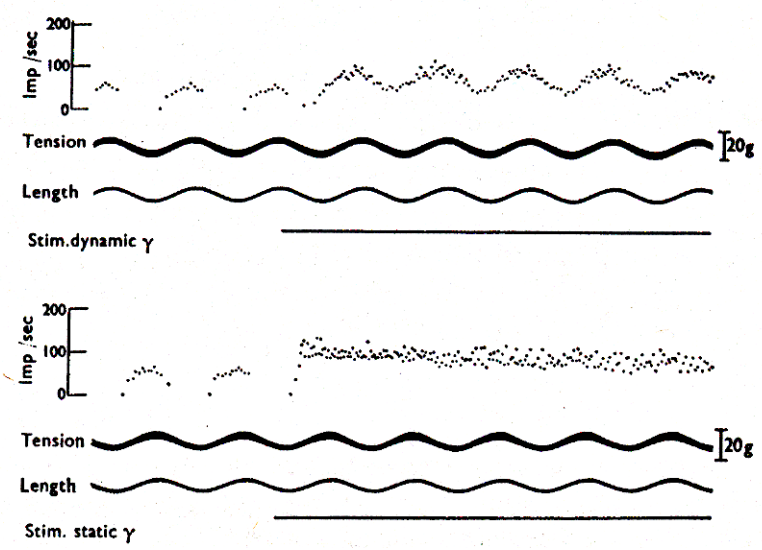

Figure 19: Effect of fusimotor activity on primary during operation mostly within the linear range. The mechanical stimulus was 0.1 mm peak-to-peak at a frequency of 2 Hz. The dynamic fusimotor stimulation was applied at 100 APs/sec. The static fusimotor stimulation was at 50 APs/ sec. The reference source did not say whether or not a static force was applied to the muscle in order to position it within the linear range of operation except during the upswing of the mechanical stimulus.

Here we have the interesting result that dynamic fusimotor stimulation removed the break in firing during negative velocities. Comparing figures 18 and 19, it is not clear what experimental conditions were different that led to the removal of the firing break. Referring back to figure 9(a), it is possible that reducing the frequency to 2 Hz sufficiently reduced the mechanical response of the fusimotor fiber to account for this difference. However, this seems unlikely to me since the amplitude of the mechanical stimulus was reduced from 1 mm peak-to-peak down to 0.1 mm peak-to-peak. Another possibility is that figure 19 might have been obtained while applying a dc stretch to make the intrafusal fibers more taut than in figure 18's case. The author (Matthew) did not state the condition, and I am inclined to suspect that the latter was the case. In any event, the characteristic firing break is present in the absence of fusimotor activity, but it is eliminated during fusimotor activity. Note that the static fusimotor stimulation was only 50 APs/sec, whereas the dynamic stimulation was at 100 APs/sec (as in figure 18). Note, too, that under dynamic fusimotor stimulation there is an obvious mix of velocity and length information (as indicated by the sinusoidal-like instantaneous frequency and by the phase shift of this response relative to the applied mechanical stimulus). There is also evidence during the dynamic stimulation of nonlinear distortion in the instantaneous firing rate response (the positive peaks are broader than the negative peaks, there is a slight "double-hump" in the positive peak, and the rising and falling edges of the instantaneous frequency response to not have the same slope).

Finally, the level of fusimotor activity affects the firing rate of the primary afferent when the muscle is at constant length. Figure 20 graphs the firing rate vs. fusimotor stimulation rate.[23] The figure illustrates that the effect on firing rate is much the same for the dynamic and the static fusimotor signals. Both curves show a gentle reduction in slope as fusimotor firing rate increases compared to the slope of the curve at low rates of fusimotor stimulation.

[23] *op. cit.*, Matthews, pg. 225.

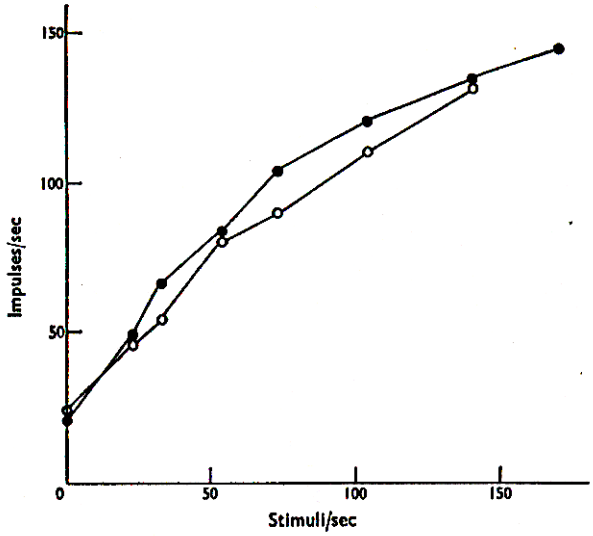

Figure 20: Effect on rate of fusimotor firing on primary spindle response at constant muscle length. The • data is for the static gamma motoneuron. The ○ curve is the data for the dynamic gamma motoneuron excitation. The presence of spontaneous firing at 0 stimulus indicates that the muscle length was such that the intrafusal fibers were taut at zero fusimotor stimulation.

As a final word on the observable properties of spindle afferent signaling, we recall that intrafusal fibers are also sometimes innervated by skeleto-fusimotor axons, i.e. by beta motoneurons. Beta motoneurons are actually nothing other than small alpha motoneurons that have the property of innervating intrafusal fibers in addition to extrafusal muscle fibers. Firing by beta motoneurons excites both the skeletomuscle fibers (acting as S-type alpha motoneurons in terms of part I of this tech brief) while at the same time exciting contraction in intrafusal fibers. Their effect on spindle afferent response is found to be the same as that produced by gamma motoneurons, but with the additional complication that the spindle afferent firing then simultaneously reflects both the mechanical muscle movement produced by the beta motoneurons as well as the modulation of the spindle firing properties produced by contraction of the intrafusal fibers. **Not every spindle is innervated by beta motoneurons**. This suggests that some spindles are electrically linked to specific motor units, while other units are "free" to be employed as needed by the spinal sensorimotor system to "instrument" movement.

IV. Transducer Mechanisms of Spindle Sensory Neurons

The experimental evidence presented in section III confronts us with some facts that do not seem to be particularly hard to understand and others that are rather puzzling. In the simple to understand category, we have the fact that secondary afferents (group II sensory neurons) appear to respond directly to changes in length of the SEC in the Hill model. While the physiological mechanism or mechanisms by which they do so may be complex, the functional description of their response seems straightforward: they fire at a rate more or less in direct proportion to x_s .

In the puzzling category we have the stunning fact that primary afferents (group Ia sensory neurons) seem to act as velocity sensors to changes of length in the SEC of bag 1 fibers, but seem to respond as length sensors to changes in x_s in the SEC of bag 2 and chain fibers. It cannot be overemphasized that this dual characteristic is found in one and the same group Ia sensory neuron (figure 11). It is as if the "bag 1 tail" of the neuron constituted one type of transducer while the "bag 2 tail" and "chain fiber tails" of this same neuron constituted a different type of transducer.

How are we to model and understand this property? How are we to quantitatively model the way in which these two types of transducers sum their responses in the sensory neuron's axon?

Near the lowest level of explanation, *all* electrical activity on the membrane voltage of a neuron is due to the opening and closing of ion channels in the membrane, and all such channels are made from proteins. It is known that some kinds of proteins implement ion channels that open and close in response to mechanical stimulation. The response of the neuron cell to ion current flow through these channels is called the *receptor potential*. Unfortunately, the means by which mechanical movement is transduced into the firing pattern of a mechanoreceptor neuron is not yet known, although it is thought that so-called "stretch activated ion channels" are responsible for the ion current to which the neuron responds.

Most mechanical transduction channels that have been studied do not respond to the absolute level of mechanical movement but rather only to relative displacements. Furthermore, most such ion channels do not maintain a response to a constant stimulus but instead "autozero" themselves so that they can respond again with full sensitivity when the mechanical displacement changes. This is called "adaptation" by the biologists. The most thoroughly studied of these kinds of channels is probably that of the hair cells of the cochlea (inner ear). (I think we all probably know that our sense of hearing responds to vibrations – i.e. "velocity" – rather than to pressure – i.e. displacement; the hair cells in our ears must "wiggle" to produce a signal). Other mechanical transduction channels do not "high pass filter" the mechanical stimulus. They maintain their signal in the presence of a constant displacement.

Now, there is no reason to presuppose that the two different "tails" of the Ia sensory neuron necessarily express the same kind of mechanosensitive ion channels. The experimental evidence reviewed earlier suggests rather strongly that these two "tails" must express different kinds of protein channels. Otherwise, bag 2 and chain fibers should show a velocity dependence and bag 1 fibers should show a position dependence that match each other quantitatively. In actuality, while it is possible that the secondary afferent and the bag 2 component of the primary afferent might each have some component of velocity dependence that is not explainable purely through the mechanical response of the Hill model, and the bag 1 component of the primary afferent might have some component of displacement, it is clear that these putative components do not come close to matching each other quantitatively in the two types of response (displacement and velocity). If a displacement response exists for bag 1 fibers and if a velocity response exists for bag 2 and/ or chain fibers, it is clear that the number of "displacement sensitive" and "velocity sensitive" protein channels must differ between the different types of sensory nerve endings. Put more succinctly, **we make the hypothesis** that the receptor potential at a nerve ending in the spindle obeys the phenomenological electromechanical relationship

$$V_r = a_1 \cdot x_s + a_2 \cdot \dot{x}_s \cdot u\left(\dot{x}_s + a_3 \cdot x_s\right) \tag{12}$$

where a_1, a_2 and a_3 are proportionality constants chosen to enforce a fit between the Hill model for each intrafusal fiber and the firing rate data given earlier. In the simplest phenomenological model, we would have $a_1 = 0$ for the bag 1 ending and $a_2 = 0$ for the bag 2 and chain fiber endings. These values would represent the extreme case where the bag 1 ending is a pure velocity transducer and the bag 2 and chain endings are pure displacement transducers. The unit step function is used to model the "cease fire" phenomenon of the primary spindle afferent during negative velocities and the a_3 term is used to model the phenomenon whereby sufficient gamma motoneuron stimulation of the bag 1 fiber combined with stretching this fiber can override the "cease fire" behavior (see figure 19).

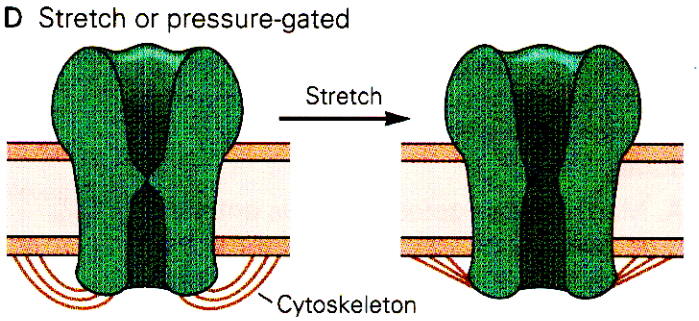

Figure 21: Conceptual model of a mechanoreceptor ion channel. In the absence of a mechanical stretch the ion channel pore is closed and no ion current can enter from outside the cell. When the cell is subjected to a stretch the pore opens, admitting cations (e.g. Na^+ or Ca^{2+}). The small filaments shown attaching to the protein act as "springs". The existence of such filaments in the case of the cochlea hair bundle has been confirmed by Pickles et al., albeit in a different arrangement than shown here.[24]

As an aid to understanding this phenomenological model, Figure 21 illustrates the putative cellular arrangement of a mechanoreceptor channel. Small filaments attaching to the channel protein serve as "springs" that pry open the channel pore when the cell membrane is stretched. This allows excitatory cation currents to flow into the membrane, raising the membrane potential. This idea seems to have been first proposed (for the case of the cochlea) by Hudsperth and his colleagues in 1983, and filaments that could play the role of springs in this model were found by Pickles et al. in 1984.[24]

How can such a model explain a velocity-sensitive mechanoreceptor? Based again on experiments involving the cochlea hair cells, Howard and Hudsperth proposed a model whereby the spring filaments are attached to a cluster of myosin motor proteins that attach the cytoplasmic side of the transduction channel to the actin core of the cell. After the channel is opened by stretching, the "spring" slowly pulls this "raft" of myosin, which slides until the channel pore is once again closed.[25] Although this model is completely hypothetical at this point, it would explain why a negative velocity apparently closes the ion channel and cuts off firing by the sensory neuron. A negative velocity moves the cytoskeleton back in the direction of the massive and slower-moving raft and "slams the door shut" (so to speak). Positive velocity, on the other hand, lets the channel pore "stay ahead of" the myosin raft and thereby stay open. It would then also follow logically that if the intrafusal fiber were sufficiently stretched, the myosin raft (which is also attached to actin filaments anchored within the cell) would not be able to move far enough to effect a closing of the channel pore. This explanation seems to be consistent with the afferent firing patterns we saw earlier.

The phenomenological model of (12) only speaks to the membrane potential at the nerve endings of the sensory neuron's axon. This must still be translated into the firing rate pattern of the sensory neuron. Here we confront another biological unknown: there are two hypotheses about where integration and firing takes place in a spindle afferent neuron and no one knows for sure which (if either) is correct. One hypothesis (with which I do not agree) argues that the firing of the sensory neuron originates right at the transducer ending where it wraps around the spindle fiber. This hypothesis also argues that the arrangement of ion channels at these endings is such as

[24] B. Hille, *Ion Channels of Excitable Membranes*, 3rd ed., Sunderland, MA: Sinauer Associates, 2001, pp. 239-248.
[25] *op. cit.*, Hille, pg. 243.

to produce a "pacemaker" mechanism (i.e. the ability to spontaneously fire). Under this hypothesis, each spindle ending could independently send its own action potentials down the axon of the sensory neuron. I do not agree with this hypothesis because there is no reason to think the axon of the sensory neuron is any different (except for the mechanotransducer channels at the nerve ending) from any other kind of axon. In a normal axon, the passing of an AP leaves behind it a refractory period during which the axon cannot conduct another AP. Referring to figure 11, this would mean that the converging APs from different spindle endings would interfere with each other at the point where the endings merge on the main axon fiber. This would produce a very complicated and irregular afferent firing pattern and the experimental data just doesn't show any such pattern.

The other hypothesis, which I and most other people agree with, is that the ion currents produced at the nerve endings sum together at or near the point where these endings converge on the main axon fiber. The trigger region of the neuron is therefore located in the main axon fiber and APs are generated at this point. In effect, this region constitutes the leaky integrate-and-fire region of the neuron.[26] This is the model we will use.

Under this model, the total stimulus arriving at the leaky integrator is proportional to the sum of the membrane potentials at each nerve ending. Because we already have phenomenological constants in (12), we can absorb the proportionality factor into these constants and write the total stimulus as

$$V_{tot} = \sum_{\forall b} V_r^{(b)} + \sum_{\forall c} V_r^{(c)} \tag{13}$$

where b is the bag fiber index and is taken over all bag fibers to which the neuron is attached, and c is the chain fiber index and is taken over all chain fibers to which the neuron is attached. The individual terms in (13) are given by (12).

In hardware we would implement (12) and (13) using our pulse-mode artificial neuron circuits. For purposes of the EC research it is simpler to merely related (13) to the firing rate of the neuron using the standard expression for firing rate in an ideal leaky integrate-and-fire neuron.[27] This expression for firing rate R is

$$R = \frac{-1/\tau_n}{\ln\left(1 - \Theta/\left(\tau_n \cdot V_{tot}\right)\right)} \cdot u\left(1 - \Theta/\left(\tau_n \cdot V_{tot}\right)\right) \tag{14}$$

where τ_n is the time constant of the leaky integrator and Θ is the firing threshold of the neuron. The constant Θ is chosen so that the firing rate "slack points" depicted in figure 14 are enforced. One numerical caution is in order here. When the unit step function in (14) is zero, this means the argument of the logarithm term is negative or zero. The argument of the step function should therefore be evaluated first and if it is negative or zero, just set $R = 0$.

---

[26] Unlike interneurons or motoneurons, the trigger region of most spiking sensory neurons is not located in the soma of the neuron. It is located in the axon near the transducer endings. The structure of most sensory neurons, including the ones we're talking about, has a long axon to which the cell body is attached by a short stub. The soma is not "in series" with the axon fiber. The axon protrudes in two directions, one leading to the transducer end, the other to its presynaptic terminals within the spinal cord. The soma itself resides in the dorsal root ganglion.

[27] J.A. Anderson, *An Introduction to Neural Networks*, Cambridge, MA: The MIT Press, 1995, pp. 52-54.

V. The Bag 1 Intrafusal Fiber

We must now go back and revisit an issue with the Hill model as this model pertains to bag fibers. I remarked earlier on how odd it was that the data of figure 9 seemed to be telling us that the bag and chain fibers shared the same time constants and stiffness ratios. I also remarked that this conclusion seemed to be radically at odds with the fiber contraction speed data of figure 10. I further noted the strange slope change in the primary data in figure 9(a). These things cannot be left as they presently are. We will take up the contraction speed problem in the next section. In this section we will deal with the "kink" in the primary curve in figure 9(a).

The response curve of figure 9(a) is a decibel plot of firing rate as a function of the mechanical frequency at which the system was being driven. Thus, the abscissa plots

$$R_{dB} = 20 \cdot \log_{10}(R).$$

What does this response look like if the neuron excitation V_{tot} is given by a sum of terms involving length and velocity sensing transducers as in (12)? This is going to depend on the mechanics of the Hill model, and this will also depend on the mechanical driving frequency ω. Consider the transfer function (10) under conditions where the Q_C term is negligible. For $\omega < \omega_z$ [28] the displacement term x_s is going to be independent of frequency and the velocity term $\dot{x}_s$ is going to be proportional to ω times an amplitude term, not necessarily of the same order as the one for x_s. This region of the curve of figure 9 is a very low frequency region, and we may therefore suppose that at very low excitation frequencies the contribution of the bag 1 velocity sensor to (13) may be insignificant compared to the displacement terms. Hence R will be independent of frequency in this range and the R_{dB} curve will be flat.

Now let us suppose that the bag 1 and bag 2 fibers differ from each other such that the zero frequencies of each stand in relation to one another as

$$(\omega_z)_{b2} < (\omega_z)_{b1}$$

where the subscripts refer to bag 2 and bag 1 sensors, respectively. This could occur, for example, if the bag 1 fiber had a smaller damping coefficient or a larger PEC stiffness or both than the bag 2 fiber. Then for frequencies in the range

$$(\omega_z)_{b2} < \omega < (\omega_z)_{b1}$$

the mechanical response of the Hill model has a +20 dB/decade slope for the bag 2 fiber while the response of the bag 1 fiber is still flat. A +20 dB/decade slope in this frequency range makes the mechanical response of the bag 2 fiber behave like a differentiator. Consequently, all the terms in (13) are going to be proportional to ω. Therefore,

[28] In Laplace transform notation, $s = j\omega$ where $j = \sqrt{-1}$. The magnitude response is given by the ratio of the magnitude of the complex numbers in the numerator and denominator of (10).

$$R_{dB} \approx 20 \cdot \log_{10}\left(\frac{-1/\tau_n}{\ln\left(1 - \frac{\zeta}{b \cdot \omega}\right)} \right)$$

where b and ζ are some constants.

As the frequency continues to increase, we come to the point where

$$(\omega_z)_{b1} < \omega < \omega_p$$

and in this region the displacement term in (13) is still proportional to ω, but now the bag 1 fiber is also acting as a differentiator. Consequently, the velocity term is now proportional to ω^2. Still ignoring the Q_C term in (10) and letting the ratio of the sensitivity of the velocity transducer to the total sensitivity of the displacement transducers be denoted as r, (10) gives us

$$\frac{V_{tot}}{\Lambda} = \frac{1}{\omega_p}\left[j\omega + (\omega_z)_{b2} + j\omega \cdot r \cdot \left(j\omega + (\omega_z)_{b1} \right) \right]$$

for $\omega < \omega_p$. In the sinusoidal steady state this gives us

$$|V_{tot}| = \frac{\lambda_{\max}}{\omega_p} \sqrt{r^2\omega^4 + \omega^2 \left[\left(1 + r \cdot (\omega_z)_{b1}\right)^2 - 2r \cdot (\omega_z)_{b2} \right] + (\omega_z)_{b2}^2} \qquad \text{(15a).}$$

Letting V denote the square root term in (15) and applying this to (14) gives us

$$R_{dB} = 20 \cdot \log\left(\frac{1}{\tau_n} \right) - 20 \cdot \log\left[-\ln\left(1 - \frac{d}{V}\right) \right] \qquad \text{(15b)}$$

where

$$d = \frac{\Theta \cdot \omega_p}{\lambda_{\max} \tau_n} \qquad \text{(15c).}$$

(15b) is plotted in Figure 22 on a normalized frequency axis (100 Hz at ω = 1) with the response normalized to give 0 dB at ω = 0.001. Parameters r and d were adjusted to obtain the best fit to the data of figure 9a. The normalized parameters correspond to $r = 2\pi \cdot 1000$ and

$$\frac{\Theta}{\lambda_{\max} \tau_n} = 0.40 .$$

The theoretical curve matched the data in figure 9a to about 1 dB over the range of the curve. Note the rolloff in the response below 0.2 Hz in the figure. This corresponds to the rolloff at low frequencies seen in figure 9a. This low frequency rolloff is primarily determined by d. Figure 23 gives the theoretical response of the secondary. This is obtained by setting the velocity transducer

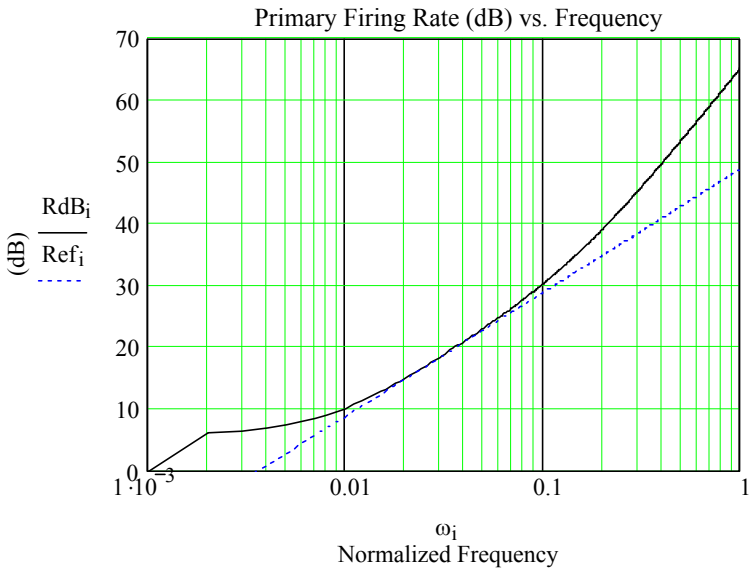

Figure 22: Plot of R_{dB} vs. normalized frequency. ω = 1 corresponds to 100 Hz. Parameters were fitted to obtain a good match to the primary response in figure 9a. The curve corresponds to $(\omega_z)_{b2}$ = 1.4 Hz and $(\omega_z)_{b1}$ = 6.3 Hz. Normalized *r'* = 10 and normalized *d'* = 0.40. The curve fits the data of figure 9a to about 1 dB (12% relative error) throughout the frequency range. The dotted line is a 20 dB/decade reference slope showing the departure in the response at higher frequencies. Note the low frequency rolloff below 0.2 Hz. The slope of this rolloff is primarily determined by *d'*.

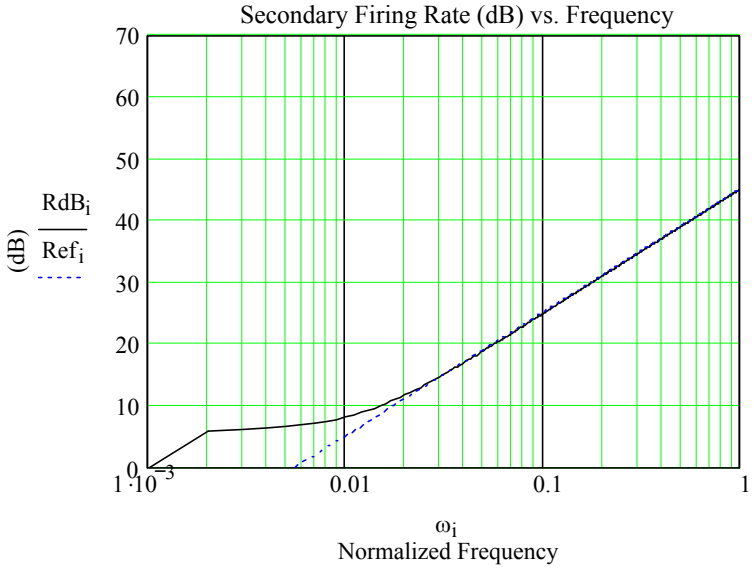

Figure 23: Plot of R_{dB} for the secondary afferents vs. normalized frequency. This plot is obtained by setting the velocity sensitivity *r* = 0. All other parameters are the same as in figure 22.

sensitivity *r* = 0. This curve also agrees with the data of figure 9a, again up to an arbitrary gain factor. Note that for the secondary the slope is a nearly perfect +20 dB/decade.

The theoretical conclusion that follows from this is that the anomalies in figure 9 are due to the integrate-and-fire characteristics of the sensory neuron and require no nonlinear modifications to the Hill model. The low frequency slope remarked upon by Matthews and Stein is real and is due to the so-called "type 2" response of the neuron.[29] The bag 1 zero frequency was fitted at 6.3 Hz (compared with 1.4 Hz for the bag 2 zero), which indicates a stiffness ratio for the bag 1 fiber of

$$\sigma_{bag1} \approx 0.067$$

compared to 0.014 for the bag 2 and chain fibers (assuming the same ω_p in both cases). The sensitivity of the velocity transducer is extremely large compared with that of the displacement transducer, the fit requiring the r value given above to be more than 3 orders of magnitude greater than that of the primary displacement transducer.

The absolute values of the frequency response characteristics under this model are determined by the time constants of the primary and secondary sensory neurons. The data of figure 9(a) indicates that the primary sensitivity at low frequencies exceeds that of the secondary by a factor of about 16.5 times, which implies that the time constant of the secondary afferent neuron is larger than that of the primary afferent neuron by 16.5 times. This in turn implies from (15c) that the threshold of the secondary afferent neuron is lower than that of the primary afferent neuron by this same multiplicative factor since d was held constant in the two figures above.

VI. Response Time of the Contractile Element

As we have noted earlier, the mechanical time constant for the Hill model is a surprisingly rapid 1.5 msec (from the data of figure 9). Yet it is also true that under motoneuron excitation the contraction of the intrafusal fibers is significantly slower than this, and the bag fibers contract more slowly than do the chain fibers. If the cause of this discrepancy cannot be laid at the doorway of the Hill model, then the only place we have left to seek it is in the parameters of the dynamical equation for $Q_C(t)$.

Motoneuron axons innervate the intrafusal tissues, and action potentials propagated down the axon induce an electrical response in the muscle fibers in much the same way that APs induce post synaptic potentials in neurons. There is, however, a significant difference in the way bag fibers and chain fibers respond electrically to these signals.

There are two "pure" ways for electrical signals to move through electrically-active tissues. One is by electrotonic passive spread, the other is by the all-or-nothing regeneration of impulses such as in the case of the axon of a neuron propagating an action potential. Electrotonic spreading is generally the slower process, resembling the distributed voltage response obtained when a pulse is applied to a ladder network of series resistors and shunt capacitors.

It is now thought that the electrical response of bag fibers (both types) is mediated by electrotonic spread, while in chain fibers the electrical response more closely resembles the propagation of an action potential.[30] This would seem to be a sufficient reason for chain fibers to contract more rapidly than bag fibers because the activation of the contraction mechanism is more

[29] W. Gerstner and W. Kistler, *Spiking Neuron Models*, Cambridge, UK: Cambridge University Press, 2002, pp. 80-82.
[30] G.M. Shepherd, *Neurobiology*, 3rd ed., NY: Oxford University Press, 1994, pg. 301.

rapidly distributed throughout the length of the intrafusal muscle fiber, thereby activating more of the contractile proteins and more quickly generating a contraction force in the muscle. Electrotonic spreading, on the other hand, takes longer to register its effects throughout the muscle, thus taking longer in order to generate the contractile force.

There also appears to be a difference in the character of electrotonic spread between bag 1 and bag 2 fibers. In an experiment by Bessou and Laporte in 1965, stimulation of dynamic gamma motoneurons produced very localized end plate potentials in bag 1 fibers.[31] Measured end plate potentials for single APs appeared to have time constants on the order of about 5 msec and appeared to be restricted to within about 0.5 mm of the endplate. Furthermore, it seems to usually be the case that gamma motoneuron endings tend to be somewhat highly localized within bag fibers, as illustrated in Figure 24.[32] This being the case, to me this seems to suggest that the buildup of contractile force Q_C throughout the muscle would likely be a process that involved the metabotropic diffusion of calcium release, and if this is so the time constant for Q_C could be significantly slower than the endplate time constant. The responses exhibited in figure 10 suggest that this time constant could be as large as about 200 msec, although the conditions of the experiment make it possible that the actual time constant might be somewhat less than this.

In the case of bag 2 fibers, Bessou's and Laporte's experiment indicated a very different characteristic endplate response. Their measurements showed a somewhat complex endplate potential able to spread to about 1 mm on either side of the endplate. One possibility that has been suggested for this more complex response is that it may be in part electrotonic and in part action-potential-like. If so, bag 2 fibers might contract more rapidly than bag 1 fibers because the effective time constant for Q_C should be smaller. However, I have no data that indicates any significant difference between contraction rates of bag 1 and bag 2 fibers, and there is data to the contrary. Figure 25 illustrates the firing rate response of a primary afferent upon being stimulated by gamma motoneuron bombardment.[33] The contractile time constant for the bag 1 (dynamic) and bag 2 (static) fibers can be estimated from the risetime of the primary firing rate. I can detect no significant difference in these two rates, and the data is consistent with a contractile time constant for bag fibers of about 125 msec.

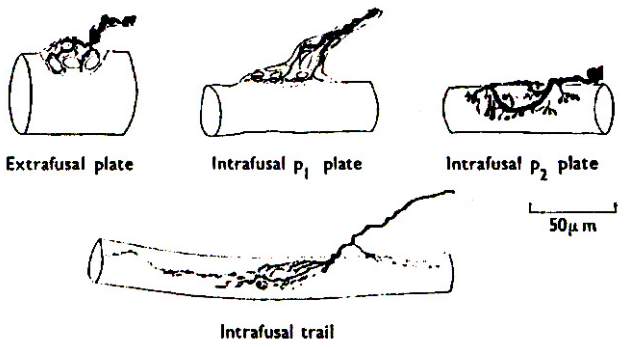

Figure 24: Sketches of various types of motor endings in muscles. The three cases at the top of the figure are for extrafusal plate endings and two types of plate endings most commonly found in bag fibers. The bottom sketch illustrates the type of motor ending most commonly found in chain fibers.

[31] *op. cit.* Matthews, pp 231-233.
[32] *op. cit.* Matthews, pg. 36.
[33] *op. cit.* Matthews, pg. 212.

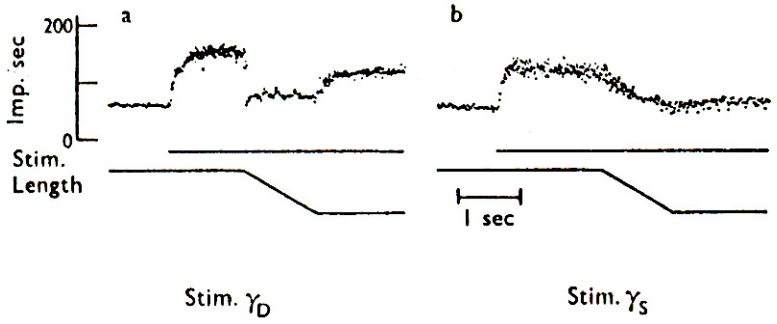

Figure 25: Change in primary afferent firing rate during stimulation by gamma motoneurons. Stimulation was at 70 pulses per sec during the bar. Time constants for Q_C can be estimated from the risetime of the response of the primary afferent firing rate. Within the resolution made possible by this graph, I can detect no significant difference in the time constants. The risetime data indicates a contractile time constant on the order of about 125 msec.

This being the case, figure 10 then suggests that the contractile time constant for the chain fiber should be about 5/12 of this value or 52 msec. These time constants are sufficiently slow at a sampling rate of 10 msec to permit numerical evaluation of the dynamical equation for Q_C by the same method as used in part I of this tech brief.

VII. Conclusion

This concludes this tech brief. We have obtained dynamical equations and parametric data for the terms in these equations based upon what we may regard as typical biological values. In order to apply our work to the BAN and Frenzel neuron hardware, we will undoubtedly need to do some frequency scaling at some point because the time scale of operation of these neurons is much faster than their biological counterparts, but this should not present any special difficulties. We should be able to use these models and these typical parameters in our EC work to come up with appropriate spinal cord neural network designs. There are a few constants, e.g. as in (12), where I have not carried through on coming up with specific numbers. However, in these cases I believe the appropriate values are implicit in the other parameters, and in some cases it may be desirable to allow our EC algorithms to determine these undetermined coefficients.

I have employed the simple type-2 integrate-and-fire model for the sensory neurons, and I think this is appropriate for our EC work. The BAN sensory neurons being developed by Ben and Dave are type-2 I&F neurons, and so EC results based on this sensory neuron model should be appropriate for our hardware network designs.